J. Fluid Mech. (1994), *vol.* 274, *pp.* 293–337

The asymptotic study of dissipation and breakdown of a wing-tip vortex

By V. N. TRIGUB, A. B. BLOKHIN AND I. N. SIMAKIN†
INTECO srl., Via Mola Vecchia 2A, I-03100 Frosinone, Italy

(Received 2 October 1992 and in revised form 11 March 1994)

The steady axisymmetrical wing-tip vortex is studied in this paper by means of asymptotic methods within the limit of high Reynolds numbers. The smooth regrouping of the vortex under the action of viscous forces is described by a quasi-cylindrical approximation. The solutions of the quasi-cylindrical approximation are thoroughly analysed numerically and it is shown that a saddle-point bifurcation appears at certain critical values of circulation. At these values the solution may be continued in two ways: as a supercritical branch which approaches the Batchelor limit far downstream; and a subcritical one, which passes the second, nodal-point bifurcation. The parabolic quasi-cylindrical equations past this point allow the downstream disturbances to propagate upstream, like for example, boundary-layer equations in the regime of strong hypersonic interaction. The flow past the second bifurcation point was studied numerically and it was shown that solutions of the quasi-cylindrical approximation with large reversed-flow regions exist. An asymptotic expansion of such solutions far downstream was constructed, and it turned out that the reversed-flow region expands exponentially. This process is halted by elliptical effects in the external flow. An asymptotic theory of large reversed-flow regions is suggested including viscosity and elliptical effects. Numerical solutions for unbounded vortex breakdown parabolically expanding far downstream are presented. Then the general asymptotic problem statement which describes the flow near the bifurcation points is used to study the asymptotic solutions near the first bifurcation point. The problem is investigated numerically and two kinds of solution, which may be treated as transcritical jumps and marginal vortex breakdown, are found and discussed.

1. Introduction

Vortex breakdown was first observed by Peckham & Atkinson (1957) in their experiments with concentrated vortex cores shed by the leading edge of the Gothic wing. A stagnation point appears suddenly in the vortex core as the angle of attack increases and the flow downstream immediately becomes unsteady and irregular. The lift drops drastically and an asymmetrical rolling moment appears which may result in a loss of control. Vortex breakdown is a phenomenon which prevents aircraft with moderately swept wings from operating at high angles of attack. For this reason much experimental engineering research is carried out on vortex breakdown near the wings of aircraft, with the aim of predicting its occurrence and its influence on the performance of an aircraft.

Vortex breakdown may also be responsible for the transmission of energy from large to small scales in turbulent flows. The visualization of turbulent flows obtained by

† I. N. Simakin died in an accident at the end of 1992.

means of direct numerical simulation shows that the bursting of the strong longitudinal vortices formed near the wall is like vortex breakdown and effectively pumps energy to small-scale motion.

The vortex structure near the wing is three-dimensional and too complicated for detailed 'clean' experimental and theoretical studies. Most of the theoretical and 'clean' experimental works deal with vortices in tubes or isolated vortices. Comprehensive reviews of these works have been done by Hall (1972) and Leibovich (1978, 1984). This paper reviews and discusses only those studies which concern our work directly.

In Leibovich & Kribus (1990), a general approach to vortex breakdown studies was suggested. The process was divided into three elements which are studied separately and then recombined. The first element is the large-amplitude axially symmetric waves in vortical flows, and this element was investigated in the paper just mentioned. The second is loss of stability to asymmetric perturbations. The third element involves effects engendered by axial inhomogeneity caused by the global flow field. The former two concern properties of the waves, while the third primarily concerns the properties of the wave guide.

We agree that these elements are the most important in comprehending the phenomenon, although we see many problems in their recombination. For this reason our approach to the study of vortex breakdown is different.

For this paper we chose the simplest but quite realistic flow in which vortex breakdown appears and we performed an asymptotic study of the flow at the limit of high Reynolds number. The analysis and synthesis are closely connected in the asymptotic study. Real elements of the phenomenon may be extracted from these studies, i.e. mathematical statements of the problems in the different regions emerging at the limit. This work contributes to a better understanding of vortex breakdown and allows one to correctly formulate mathematical statements of the problems for the next stage – direct numerical simulation of vortex breakdown.

As noted by Hafez *et al.* (1987): 'Perhaps the single most important contribution to the study of the vortex breakdown was made by Harvey (1962), who isolated the vortex from the wing...'. In our work we also isolate the vortex from the tube and study the single trailing wing-tip vortex. Morton (1969) pointed out that single unbounded vortices of this type cannot be generated because they would require infinite kinetic energy and would also have infinite angular momentum. Therefore, such vortices do not actually occur singly but in pairs. For these vortices in pairs, with equal and opposite circulation, the kinetic energy is finite and the angular momentum is zero. We study the flow far enough from the wing but close to one of the vortices so that effects of the second are negligible.

Trailing wing-tip vortices are well-known because often, owing to condensation of vapour, they are highly visible in the sky as very long tails at the rear of the plane. The study of their breakdown is also a problem of practical interest and concern since these vortices behind large aircraft represent substantial danger for other aircraft. There is particular concern in airport zones where many large aircraft are in continuous movement simultaneously.

Theoretical studies of trailing tip vortices include those of Batchelor (1964), Gartshore (1963), Mager (1972), Lessen, Singh & Paillet (1974) and Lessen & Paillet (1974). In Batchelor's (1964) work the correct asymptotic expansion for a dissipating trailing vortex far from the aircraft was obtained. Gartshore (1963) studied the quasi-cylindrical approximation for a trailing vortex using an integral approach. He found that a singularity may appear in the course of integration of the equations and the

solution cannot be continued beyond the singular point. He suggested that these singularities may be mathematical indications of vortex breakdown. This work was continued by Mager (1972) who also used the integral approach to solve equations of the quasi-cylindrical approximation. He made an attempt to connect the solutions obtained with the concept of the breakdown as a supercritical–subcritical jump suggested by Benjamin (1962). The inviscid and viscous stability of a vortex which has an asymptotic structure obtained by Batchelor (1964) was studied in the papers of Lessen *et al.* (1974) and Lessen & Paillet (1974). We are not aware of any current asymptotic studies of the trailing vortex breakdown at the limit of high Reynolds numbers discussed here.

The traditional objection to such an approach is that the real flow at high Reynolds number is turbulent. Nevertheless, we believe that understanding the vortex breakdown mechanisms obtained in asymptotic studies of laminar flow is helpful in dealing with turbulent flow too.

The plan of the paper is as follows. The general formulation of the problem and its statement at the limit of the quasi-cylindrical approximation are described in §2. The probe function is constructed which indicates remoteness of the vortex state from critical, bifurcation conditions. Two integral invariants are given and the asymptotic expansion obtained by Batchelor (1964) is completed by additional terms depending on the invariant of angular momentum deficiency. A numerical study of the solutions in the quasi-cylindrical approximation is performed; two types of bifurcation points are found. An unexpected result is obtained: the solutions pass the second bifurcation point regularly. The connection between singularity, bifurcations and the condition of criticality is discussed.

An asymptotic theory of the flow near the bifurcation points is formulated in §3. Governing equations are obtained and all possible types of bifurcations are indicated. Calculations are performed to understand which types were observed in previous numerical solutions. It was found that the first bifurcation has a saddle-point structure, while the second has a nodal-point structure. This means that the parabolic equations of the quasi-cylindrical approximation past the second bifurcation point allow the downstream disturbances to propagate upstream.

The solutions of the quasi-cylindrical approximation past the second bifurcation point are studied numerically in §4. It is shown that solutions with large reversed-flow regions exist. Then the asymptotic expansion of the solution far downstream is constructed. It turns out that the reserved-flow region expands exponentially. This process is halted by elliptical effects in the external flow.

The asymptotic theory of the large reversed-flow regions which include the action of viscosity and elliptical effects is formulated in §5. Governing equations and scaling are derived and numerical solutions for unbounded vortex breakdown parabolically expanding far downstream are obtained.

In §6 we return to the asymptotic equations describing the flow near the first bifurcation point, which were obtained in §3. The problem is studied numerically and two types of solutions, which can respectively be treated as transcritical jumps and marginal vortex breakdown, are found and discussed.

2. Smooth, singular and bifurcating solutions of the quasi-cylindrical approximation

2.1. *Problem formulation*

We shall consider a steady axisymmetrical trailing wing-tip vortex which is surrounded by infinite potential flow with uniform velocity $u_{\infty d}$ and circulation $g_{\infty d}$ far from the vortex. We shall introduce a cylindrical coordinated system (x_d, r_d) with the x_d-axis directed along the vortex axis in the downstream direction. The axial, radial and azimuthal components of velocity and pressure are u_d, v_d, w_d, p_d respectively. The fluid is considered to be incompressible with constant density ρ_d (index d denotes dimensional values).

First, we shall investigate the slow regrouping of the internal vortex structure due to the effects of viscous forces up to the state described by the expansions of Batchelor (1964).

If the derivative $\mathrm{d}r_d/\mathrm{d}x_d$, where r_d is the radius of the vortex core, is small the main approximation for the velocities in the potential flow is (Goldstein 1960, pp. 181–195)

$$u_d = u_{\infty d} - \frac{u_{\infty d}}{4\pi}\int_{-\infty}^{+\infty} \frac{\mathrm{d}^3 S_d}{\mathrm{d}\lambda_d^3} \ln\left(2\frac{|x_d-\lambda_d|}{r_d}\right)\mathrm{sgn}\,(x_d-\lambda_d)\,\mathrm{d}\lambda + \ldots, \tag{2.1a}$$

$$v_d = u_{\infty d}\frac{1}{2\pi r_d}\frac{\mathrm{d}S_d}{\mathrm{d}x_d} + \ldots, \quad w_d = \frac{g_{\infty d}}{r_d} + \ldots. \tag{2.1b, c}$$

Here S_d is the distribution of sources along the axis which is determined by the form of the vortex radius variation. It is supposed that the third derivative of the function S_d decays at infinity rapidly enough to provide convergence of the integral.

If we suppose that only viscous forces change the vortex core we can find the asymptotic expansion of the functions inside the core in the form

$$u_d = u_{\infty d}(u(x,y) + O(\mu^*)), \tag{2.2a}$$

$$v_d r_d = \epsilon u_{\infty d} r_{0d}(v(x,y) + O(\mu^*)), \tag{2.2b}$$

$$w_d r_d = u_{\infty d} r_{0d}(g(x,y) + O(\mu^*)), \tag{2.2c}$$

$$p_d = \rho_d u_{\infty d}^2 (p(x,y) + O(\mu^*)), \tag{2.2d}$$

where $x = \epsilon x_d/r_d$; $y = \frac{1}{2}(r_d/r_{0d})^2$; $\epsilon = \nu_d/u_{\infty d} r_{0d}$; ν_d is the coefficient of viscosity; r_{0d} is the characteristic radius of the vortex core at the initial position; and $\mu^* = \epsilon^2 \ln(1/\epsilon)$. Second-order terms of $O(\mu)$ are caused by interaction of the vortex with the external potential flow.

Taking the limit $\epsilon \to 0$; $x, y = O(1)$ in the Navier–Stokes equations, we obtain the quasi-cylindrical approximation (Gartshore 1963; Hall 1967)

$$u\frac{\partial u}{\partial x} + v\frac{\partial u}{\partial y} = -\frac{\partial p}{\partial x} + 2\frac{\partial}{\partial y}\left(y\frac{\partial u}{\partial y}\right), \tag{2.3a}$$

$$u\frac{\partial g}{\partial x} + v\frac{\partial g}{\partial y} = 2y\frac{\partial^2 g}{\partial y^2}, \tag{2.3b}$$

$$\frac{\partial p}{\partial y} = \frac{g^2}{4y^2}, \quad \frac{\partial u}{\partial x} + \frac{\partial v}{\partial y} = 0. \tag{2.3c, d}$$

System (2.3) is nonlinear parabolic, just like the system of boundary-layer equations. Generally, natural boundary conditions for (2.3) are:

$$x \geqslant 0, \quad y \geqslant 0; \tag{2.4a, b}$$

$$u(0,y) = u^0(y), \quad g(0,y) = g^0(y); \tag{2.4c, d}$$

$$u(x,y) = 1 + O(\exp), \quad g(x,y) = g_\infty + O(\exp), \tag{2.4e, f}$$

$$p = p_\infty + O(y^{-1}) \quad \text{as} \quad y \to \infty; \tag{2.4g}$$

$$g(x,0) = 0, \quad v(x,0) = 0, \quad |u(x,0)| < \infty, \tag{2.4h–j}$$

where $O(\exp)$ are the terms which decay exponentially as $y \to \infty$; g_∞, p_∞ are constants. The last condition means that axial velocity is finite at $y = 0$.

System (2.3) may also be represented in the form 'resolved relatively x-derivatives'.

$$v'' - R_1(u,g)\,v = D_1(u,g), \tag{2.5a}$$

$$\frac{\partial u}{\partial x} = -v', \quad \frac{\partial g}{\partial x} = -\frac{v}{u}g' + \frac{2y}{u}g'', \tag{2.5b, c}$$

$$R_1 = \frac{u''}{u} - \frac{gg'}{2y^2u^2}, \quad D_1 = \frac{g''}{yu^2} - \frac{2(yu')''}{u}, \tag{2.5d, e}$$

where the prime denotes derivatives in the radial direction.

This form is suitable for analysis and for numerical calculations of vortices without stagnation points ($u > 0$). If the u, g profiles are known at some position $x = x_0$ the functions R_1, D_1 may be calculated and the function v may be obtained by solving the non-homogeneous linear equations (2.5a) with boundary conditions $v(x_0, 0) = 0$, $v'(x_0, \infty) = 0$. Then the u, g profiles may be continued further using (2.5b, c). Equation (2.1a) cannot be solved if the boundary-value problem for the related homogeneous equation

$$\phi_0'' - R_1\phi_0 = 0, \quad \phi_0(0) = 0, \quad \phi_0'(\infty) = 0 \tag{2.6a, b}$$

has a solution. It was shown by Trigub (1985a) that in this case the solution of (2.5) is singular at the point x_0: $v \sim \partial u/\partial x \sim \partial g/\partial x \sim O((x_0 - x)^{1/2})$; and cannot be continued beyond the point x_0. The only exception is when the additional solvability condition

$$\int_0^\infty D_1\phi_0\,\mathrm{d}y = 0 \tag{2.7}$$

is satisfied. In this case the point $x = x_0$ is a bifurcation point for problem (2.5) and generally there are two regular solutions of (2.5) which originate from this point.

More complex singularities and bifurcations may appear if additional conditions are satisfied for the u and g profiles. The situations were also analysed by Trigub (1985a) but we are not concerned with them in the present work since only the most general singularities and bifurcations (mentioned above) were encountered in our calculations.

Two conservation laws found by Gartshore (1963) are satisfied for problems (2.3) and (2.4). In Gartshore (1963) and Mager (1971, 1972), the integration was performed up to the finite radius of the vortex core so that the flow force-deficiency conservation law contained this radius. We obtained this law in another form independent of that artificial value. Integration of (2.3) using boundary conditions (2.4) yields after considerable manipulation

$$\int_0^\infty (u(1-u) - \tfrac{1}{2}gg' \ln y)\,\mathrm{d}y = C_2, \tag{2.8a}$$

$$\int_0^\infty u(g_\infty - g)\,\mathrm{d}y = 2g_\infty x + C_1, \tag{2.8b}$$

where C_1 and C_2 are constants which are determined by initial profiles $u^0(y), g^0(y)$. Using Mager's (1972) definitions, C_1 is called the invariant initial value of the flux of the angular momentum deficiency and C_2 the invariant flow force deficiency.

It was shown by Batchelor (1964) that an arbitrary constant which appears in his asymptotic expansion of a solution of (2.3) and (2.4) far downstream depends on the invariant C_2 only. Therefore, another arbitrary constant must exist in the expansion which depends on C_1. We extended the expansions and found terms which contain this invariant. The expansions may be represented as

$$u = 1+\frac{\ln x}{x}u_{10}(\eta)+\frac{1}{x}[\tfrac{1}{8}g_\infty^2 u_{11}(\eta)+a\,\mathrm{e}^{-\eta}]+O^*\left(\frac{1}{x^2}\right), \tag{2.9a}$$

$$g = g_0(\eta)+\frac{\ln x}{x}g_{10}(\eta)+\frac{1}{x}[\tfrac{1}{16}g_\infty^3 g_{11}(\eta)+b\eta\,\mathrm{e}^{-\eta}]+O^*\left(\frac{1}{x^2}\right), \tag{2.9b}$$

where $\eta = y/2x$,

$$u_{10} = -\tfrac{1}{8}g_\infty^2\,\mathrm{e}^{-\eta},\quad p(\eta) = \frac{1}{g_\infty^2}\int_\eta^\infty \frac{g_0^2}{\eta^2}\mathrm{d}\eta,\quad u_{11} = \mathrm{e}^{-\eta}\int_0^\eta\left[\frac{1-\mathrm{e}^{-\eta}}{\eta}+\mathrm{e}^{\eta}p(\eta)\right]\mathrm{d}\eta,$$

$$g_0 = g_\infty(1-\mathrm{e}^{-\eta}),\quad g_{10} = -\tfrac{1}{16}g_\infty^3\,\eta\,\mathrm{e}^{-\eta},\quad g_{11} = \eta\,\mathrm{e}^{-\eta}\int_0^\eta\left(\frac{\eta-1+\mathrm{e}^{-\eta}}{\eta^2}\right)\mathrm{d}\eta.$$

We use $O^*(x^\alpha)$ to denote all terms which have the form $O(x^\alpha(\ln x)^\beta)$, for all α, β.

The arbitrary constants a, b may be obtained if invariants C_1, C_2 are known:

$$a = -\tfrac{1}{2}C_2-\tfrac{1}{4}g_\infty^2\int_0^\infty\left[\tfrac{1}{2}u_{11}+\frac{1}{g_\infty^2}g_0 g_0'\ln(2\eta)\right]\mathrm{d}\eta,$$

$$b = \tfrac{1}{2}g_\infty a-\tfrac{1}{2}C_1+\tfrac{1}{8}g_\infty^3\int_0^\infty(u_{11}\,\mathrm{e}^{-\eta}-\tfrac{1}{2}g_{11})\,\mathrm{d}\eta.$$

The second and third terms in the expansion of g, (2.9b), were not considered by Batchelor (1964).

2.2. *Numerical solution*

The initial conditions were chosen from the two-parameter class of velocity and circulation profiles:

$$u^0 = 1-(1-\alpha)\,\mathrm{e}^{-y},\quad g^0 = g_\infty(1-\mathrm{e}^{-y}). \tag{2.10}$$

The velocity and circulation distributions upstream from the position of a vortex breakdown (Leibovich 1978) are approximated well by such profiles. The system 'resolved relatively x-derivatives' (2.5) was solved numerically using the high-accuracy pseudo-spectral method for calculation of y-derivatives.

The v, u, g profiles were approximated by the sums of Laguerre polynomials multiplied by exponents so that boundary conditions at $y = 0$ and as $y\to\infty$ were satisfied. The $u_i(x)$, $g_i(x)$, $i = 1, N$ at the collocation points coinciding with zeros of the Laguerre polynomials were considered as unknown functions of x. If vectors u_i, g_i are known at some position x, the y-derivatives at the collocation points may be calculated by multiplying the differentiation matrix on these vectors. The equation for v is transformed after such a procedure to a linear system of algebraic equations for v_i, $i = 1,\ldots, N$. This system is solved and the result substituted into the right-hand side of the equations for u, g. As a result, we obtain a nonlinear system of $2N$ ordinary differential equations for $u_i(x)$, $g_i(x)$ 'resolved relatively x-derivatives'. Gear's implicit method with automatic choice of x-step was used to solve the nonlinear system.

Another, quite different, numerical method for solving (2.3) and (2.4) is described in

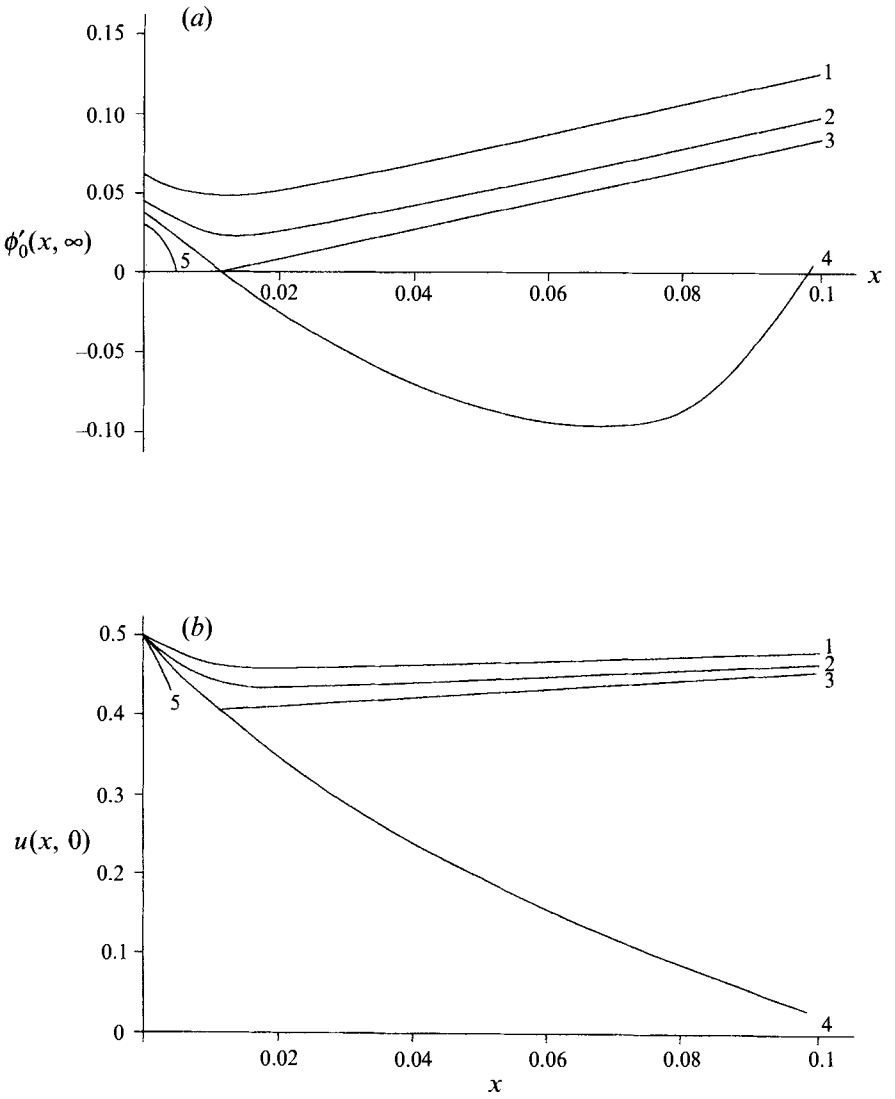

FIGURE 1. (*a*) The probe function $\phi_0'(x, \infty)$ indicating the remoteness from the critical conditions and (*b*) the axial velocity on the axis $u(x, 0)$ at $\alpha = 0.5$. Lines 1–5 correspond to $g_\infty = 1.14, 1.17, 1.18562, 1.185624, 1.2$.

§4.1. Each approach was validated by comparison with the results obtained using one approach with those from the other. To control the numerical error the invariants C_1, C_2 were calculated at each x-step. The finite results presented here were obtained with $N = 64$ polynomials. The relative changes of C_1, C_2 were smaller than 10^{-6}. All programming was performed easily using tools of the spectral-methods TURLEN Mathematical Library (Blokhin *et al.* 1992).

Equation (2.6) was used to determine the remoteness of the solution from a singularity or bifurcation. The Cauchy problem for this equation with initial condition $\phi_0(x, 0) = 0$, and normalization $\phi_0'(x, 0) = 1$ was solved at each x-step and $\phi_0'(x, \infty)$ was found. This, as noted above, must be zero at a point of singularity or bifurcation. The results of integrations for initial profiles at $\alpha = 0.5$ and $g_\infty = 1.14$, 1.17, 1.18562, 1.185624, 1.2 (curves 1, 2, 3, 4, 5, respectively) are shown in figures 1–3.

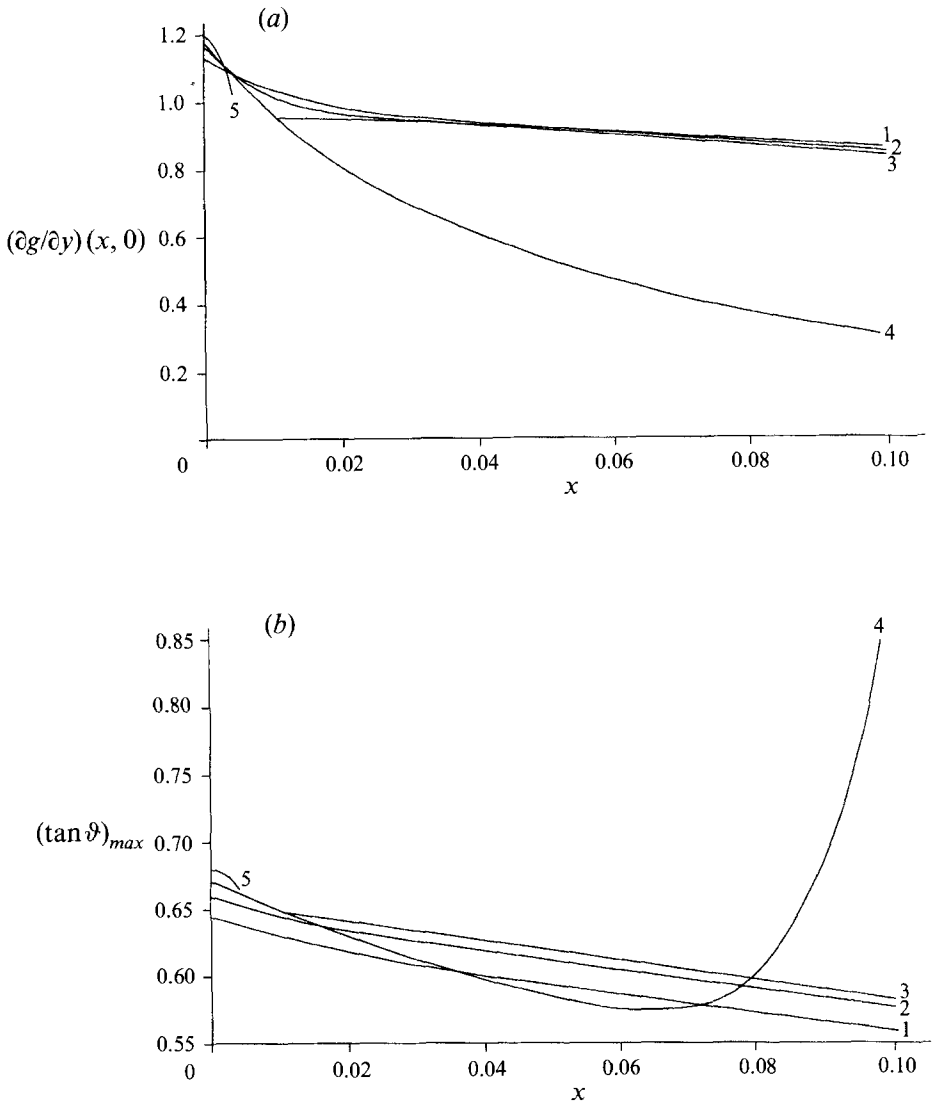

FIGURE 2. (*a*) The angular velocity of rotation near the axis and (*b*) the tangent of the maximum swirl angle at $\alpha = 0.5$. Lines 1–5 correspond to the same values of g_∞ as in figure 1.

The variations of $\phi_0'(x, \infty)$ are presented in figure 1(*a*): at small values of g_∞ it reaches a minimum and then gradually increases, approaching the asymptotic behaviour predicted by Batchelor (1964). The radius of the curve at the position of the minimum tends to zero as g_∞ approaches the critical value $g_\infty = 1.185624$ so that curve 3, obtained at a value of g_∞ very close to the critical, seems to have a sharp bend. At the critical value of g_∞ a bifurcation point appears from which two solutions originate. One of them belongs to the class approaching Batchelor's limit. This is limiting for a singular solution of this class because the normal velocity, and derivatives $\partial u/\partial x$, $\partial g/\partial x$, have a finite break at the point of bifurcation. We were also able to obtain another solution which passes the bifurcation point regularly. The value of $\phi_0'(x, \infty)$ becomes negative, reaches a minimum and then passes the bifurcation point again regularly. This was a very unexpected finding and was checked carefully.

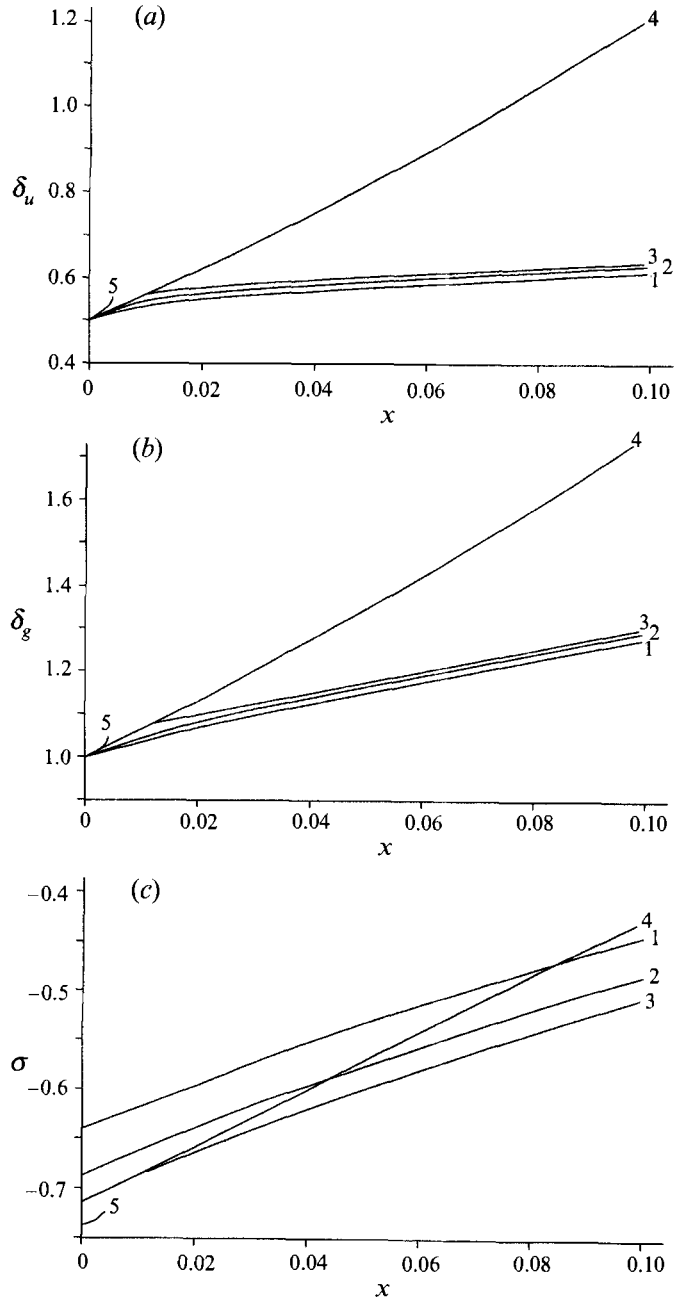

FIGURE 3. (*a*, *b*) The vortex thicknesses δ_u, δ_g, and (*c*) the stagnation pressure parameter σ at $\alpha = 0.5$. Lines 1–5 correspond to the same values of g_∞ as in figure 1.

An instability in the numerical results is manifested at some distance below the second bifurcation point – the results become dependent on the number of basic functions N and the precision of integration stated in Gear's integrator. With the method used, we were not able to obtain reliable numerical results there. We shall return to this situation in §3 to investigate the solutions of the quasi-cylindrical approximation in the vicinity of the bifurcation point analytically and continue the

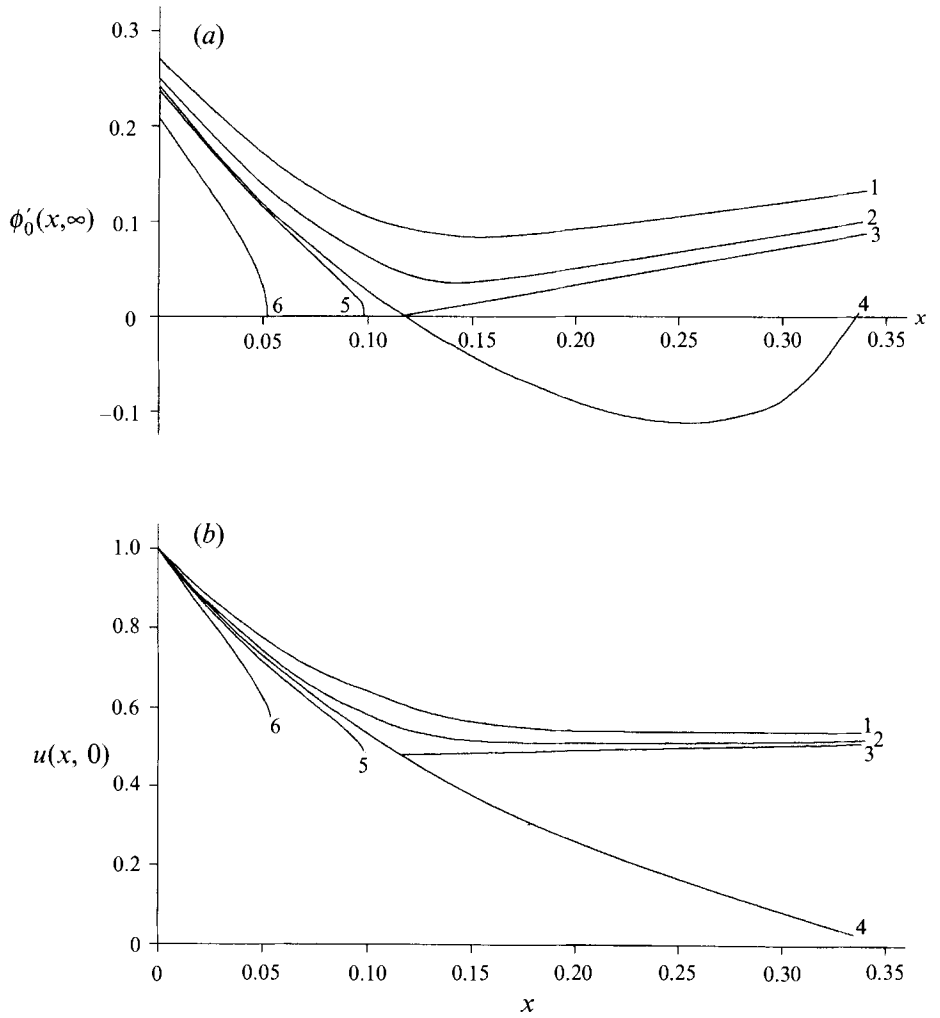

FIGURE 4. (*a*) The probe function and (*b*) the axial velocity on the axis at $\alpha = 1$. Lines 1–6 correspond to $g_\infty = 1.7$, 1.73, 1.74444, 1.74445, 1.75, 1.8.

solution numerically using another method. At values of g_∞ higher than critical, a solution is singular, at some point $x_0 (v \sim \partial u/\partial x \sim \partial g/\partial x \sim (x_0 \sim x)^{-1/2}$ as $x \to x_0)$ and cannot be continued beyond this point, as is demonstrated by curve 5.

The variations of axial velocity on the axis are shown in figure 1 (*b*). Curves 1–3 have minima (the minimum appears as a sharp bend for curve 3 and then the velocity slowly increases. The velocity decreases monotonically in the unique solution 4. The velocity at the second bifurcation point, which is located at $x = 0.09802$, is $u = 0.02736$. The singular solution 5 cannot be continued beyond the point of singularity.

The behaviour of the derivative $g'(x, 0)$ on the axis is demonstrated in figure 2 (*a*). This derivative characterizes the angular velocity of rotation near the axis. In the class of solutions 1–3, its value decreases monotonically due to viscous dissipation. It decreases much quicker on the unique solution 4. Nevertheless, the maximum swirl angle

$$\vartheta = \left(\frac{g}{(2y)^{1/2}u}\right)_{max}$$

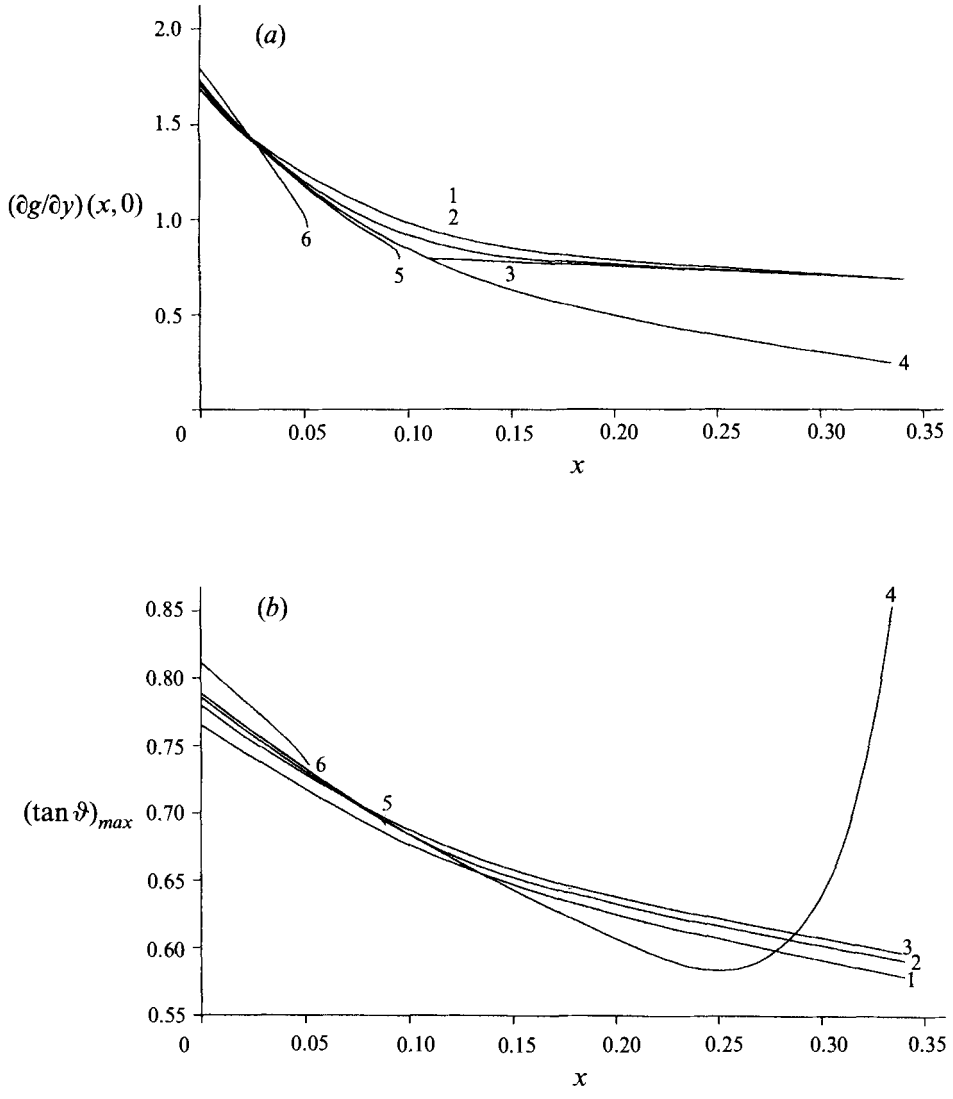

FIGURE 5. (*a*) The angular velocity of rotation near the axis and (*b*) the tangent of the maximum swirl angle at $\alpha = 1.0$. Lines 1–6 correspond to the same values of g_∞ as in figure 4.

increases very strongly near the second point of bifurcation, as shown in figure 2(*b*). This is because not only u, but also $\partial u/\partial y$ on the axis decrease. The variations of two vortex thicknesses

$$\delta_u = \int_0^\infty (1-u)\,\mathrm{d}y \quad \text{and} \quad \delta_g = \int_0^\infty (g_\infty - g)\,\mathrm{d}y$$

are represented on figures 3(*a*) and 3(*b*). The thicknesses increase monotonically for all solutions.

Parameter $\sigma = (p_{std} - p_{\infty d})/(\frac{1}{2}\rho_d u_{\infty d}^2)$, where p_{std} is stagnation pressure on the axis and $p_{\infty d}$ is pressure in the free stream, plays an important role in considerations of vortex breakdown. We shall introduce the following definition concerning steady axisymmetrical forms of vortex breakdown in theoretical models. We shall call a vortex breakdown an 'unbounded breakdown' if fluid particles from the axis of the vortex

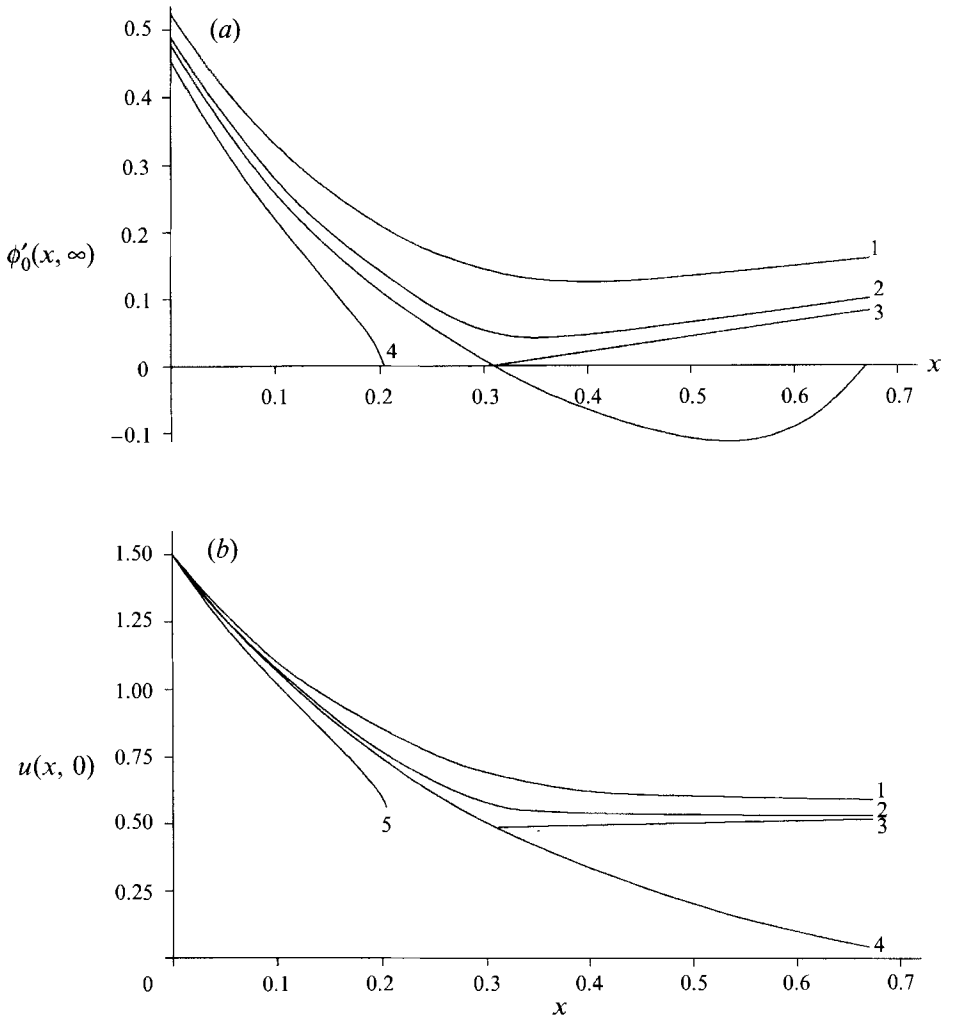

FIGURE 6. (*a*) The probe function and (*b*) the velocity on the axis at $\alpha = 1.5$. Lines 1–5 correspond to $g_\infty = 2.15, 2.2, 2.2135, 2.21353, 2.25$.

core penetrate the external potential flow infinitely far from the axis, i.e. the region of the reversed (or stagnated) flow is unbounded in the radial direction. In other cases we shall call it 'bounded'. The unbounded forms in inviscid fluid are possible only for $\sigma \geqslant 0$. An example of a vortex breakdown model in which the stagnation region is semi-infinite and has the form of a paraboloid far from the critical point where $\sigma = 0$ was suggested by Trigub (1985*b*). This model was extended recently by Vic. Sychev (1992), who took viscosity effects into consideration.

The variations of

$$\sigma = u^2(x, 0) - \int_0^\infty (g^2/2y^2)\, \mathrm{d}y$$

are shown in figure 3(*c*). We see that $\sigma < 0$ everywhere for all solutions considered.

The results of integrations at $\alpha = 1$ and $g_\infty = 1.7, 1.73, 1.74444, 1.74445, 1.75$, and 1.8 are shown on figures 4 and 5 (curves 1–6 respectively); and at $\alpha = 1.5$ and $g_\infty = 2.15, 2.2, 2.2135, 2.21353$, and 2.25 on figures 6 and 7 (curves 1–5 respectively). These results demonstrate that the behaviour of the solutions described above is not unique,

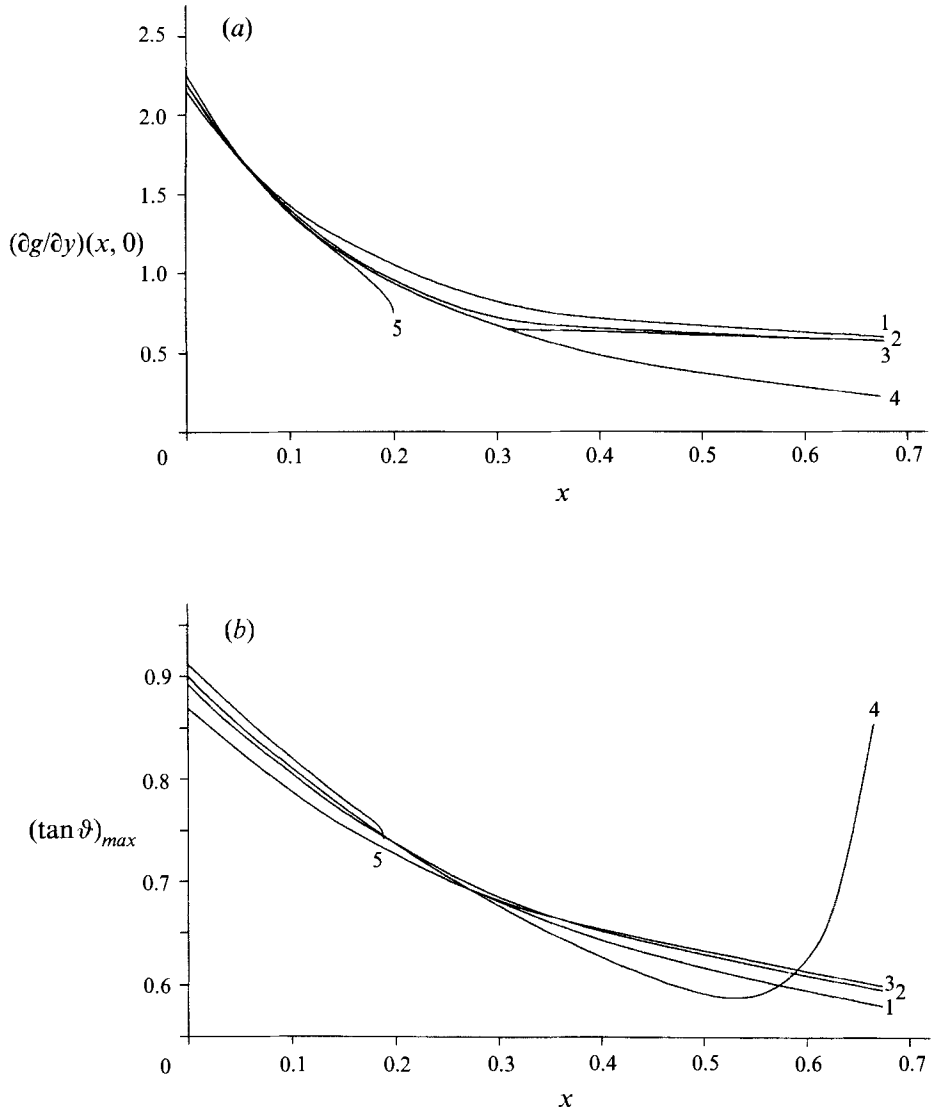

FIGURE 7. (*a*) The angular velocity of rotation near the axis and (*b*) the tangent of the maximum swirl angle at $\alpha = 1.5$. Lines 1–5 correspond to the same values of g_∞ as in figure 6.

but is similar for a wide class of velocity profiles from wake-like ($\alpha = 0.5$) to jet-like ($\alpha = 1.5$).

The most interesting solutions are those close to the unique one passing the first bifurcation point regularly. Figures 8 (*a*) and 8 (*b*) represent the dependence of both g_∞, at which the bifurcations appear, and the position of the first bifurcation point x_b on α. At an α of less than 0.4, x_b coincides with $x = 0$. As we shall demonstrate in the next subsection, at smaller values of α the initial profiles correspond to a subcritical state. These situations are not discussed in the present paper.

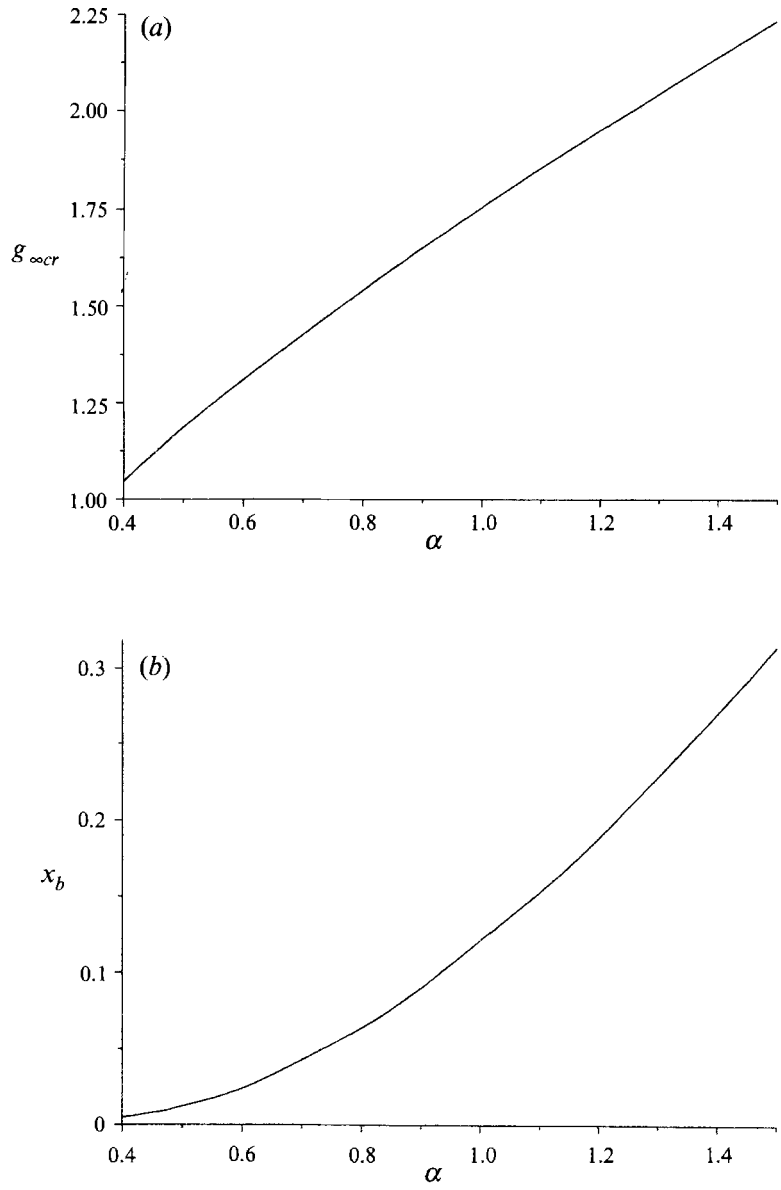

FIGURE 8. (*a*) The critical value of the circulation $g_{\infty cr}$ and (*b*) the position of the first bifurcation point x_b, versus α.

2.3. *Supercritical and subcritical states: connection with the bifurcations and singularities in the quasi-cylindrical approximation*

The classification of vortices into supercritical and subcritical for inviscid cylindrical flows was originally suggested by Benjamin (1962). It may be easily generalized to consider local properties of profiles in the quasi-cylindrical approximation. The classification is based on an analysis of small perturbations whose longitudinal scale is of the order of the vortex radius, which is much smaller than the longitudinal scale in the quasi-cylindrical approximation. Hence, the effects of viscosity are locally insignificant and the main flow is locally parallel in the limit $\epsilon \to 0$.

If small disturbances of the stream function are considered in the form

$$\exp\left[\int_0^x \Omega(\xi)\,\mathrm{d}\xi\right]\phi(y),$$

the following eigenvalue problem will be obtained after taking the limit in the Navier–Stokes equations:

$$\phi''+\left(\frac{\Omega^2}{2y}-R_1(u,g)\right)\phi=0,\quad \phi(0)=0,\quad \phi'(\infty)=0. \tag{2.11 a–c}$$

Benjamin (1962) suggested a classification for vortex flows confined in a tube. This may be generalized in the following way. We shall state boundary condition (2.11 *c*) at large, but finite distance y_B: $\phi'(y_B)=0$.

With the assumptions about u, g made above, the problem has an infinite series of real eigenvalues $\Omega_0^2<\Omega_1^2<\Omega_2^2\ldots$. If $\Omega_0^2<0$ and therefore, if the standing waves can be maintained, the state with local u, g profiles is called 'subcritical', and 'supercritical' when $\Omega_0^2>0$. As the swirl increases, Ω_0^2, Ω_1^2, etc. decrease and pass through zero, one after the other. The real eigenvalues $\Omega_i^2>0$ are condensed into a continuous spectrum $\Omega^2>0$ as $y_B\to\infty$. The corresponding eigenfunctions oscillate and slowly increase ($\phi'\sim y^{-1/4}\sin(\Omega(2y)^{1/2})$) at $y\gg 1$. However, the eigenvalues $\Omega_i^2<0$ are slightly changed and have limits as $y_B\to\infty$; the corresponding eigenfunctions decay exponentially. Therefore, the flow is 'subcritical' or 'critical' if (2.11) has solutions which decay exponentially as $y\to\infty$ (possible only if $\Omega^2\leqslant 0$). The flow is 'critical' if the solution exists only at $\Omega=0$.

Comparing (2.11) and (2.6) we find that every consecutive appearance of a zero eigenvalue Ω_k as the swirl increases will led to a singularly (or bifurcation) in the quasi-cylindrical approximation. This means that the quasi-cylindrical approximation has a singularity or bifurcation only in the vicinity of u, g profiles capable of maintaining standing waves of infinite (on the scale of the vortex core radius) length.

Eigenvalue problem (2.11) was solved numerically at each x-step during the solution of the problem (2.5). All initial profiles considered were supercritical. The critical state appears as g_∞ increases at the first bifurcation point. Two solutions originate from this critical state: the limiting singular solution, which is supercritical everywhere, and the unique solution which is subcritical. An eigenvalue $\Omega_0^2<0$ appears when this solution passes the first bifurcation point along the separation line. This eigenvalue decreases monotonically and another mode $\Omega_1^2<0$ appears after passing the second bifurcation point. Therefore, the solution is subcritical everywhere beyond the first bifurcation point with one standing wave above the second bifurcation and two waves below it. The solutions at larger values of g_∞ are supercritical and become critical at singular points. These critical states cannot be continued beyond the singularity.

For a subcritical state capable of maintaining standing waves with length comparable with the core radius, questions arise about the justification of the quasi-cylindrical approximation for such flows. We investigated this problem and found that the quasi-cylindrical approximation is also appropriate for the description of the average base flow in the presence of standing waves.

3. Study of the flow near bifurcation points in the solutions of the quasi-cylindrical approximation

3.1. *The governing equation describing the flow near a bifurcation point*

We shall study the structure of solutions near a bifurcation point. We introduce two small parameters: $\delta = g_{\infty cr} - g_\infty$, where $g_{\infty cr}$ is the value of g_∞ at which the bifurcation appears in the solution of the quasi-cylindrical approximation; and θ, the parameter, whose order will be determined below, such that $\theta \to 0$ as $|\delta| \to 0$.

It was shown that $|\partial v/\partial x|$ tends to infinity as $\delta \to 0$ near the first bifurcation point for all solutions except the unique one passing the point regularly. The quasi-cylindrical approximation ceases to be valid in the vicinity of this point at small values of δ and elliptical effects must be included. For this reason we intend that δ is a function of ϵ, $\delta \to 0$ as $\epsilon \to 0$, and consider the limit $\epsilon \to 0$ in the full Navier–Stokes equations.

We shall represent the disturbed solution near a bifurcation point in the form

$$\psi_d = u_{\infty d} r_{0d}^2 (\psi_0(y) + \theta\psi_1(X,y) + \theta^2\psi_2(X,y) + o(\theta^2)), \tag{3.1a}$$

$$u_d = u_{\infty d}(u_0(y) + \theta u_1(X,y) + \theta^2 u_2(X,y) + o(\theta^2)), \tag{3.1b}$$

$$v_d r_d = \epsilon u_{\infty d} r_{0d}(v_1(X,y) + \theta v_2(X,y) + o(\theta)), \tag{3.1c}$$

$$w_d r_d = u_{\infty d} r_{0d}(g_0(y) + \theta g_1(X,y) + \theta^2 g_2(X,y) + o(\theta^2)), \tag{3.1d}$$

$$p_d = \rho_d u_{\infty d}^2 (p_0(y) + \theta p_1(X,y) + \theta^2 p_2(X,y) + o(\theta^2)), \tag{3.1e}$$

where ψ is the stream function; $X = (x - x_b)/\theta$; x_b is the position of a bifurcation point in a solution of the quasi-cylindrical approximation.

The following procedure is similar to that suggested first by Leibovich (1970) and used by Randal & Leibovich (1973). The difference is that we study disturbances near the special critical state – the bifurcation point of the quasi-cylindrical approximation.

We shall determine $\epsilon^2/\theta^3 = O^*(\epsilon^0)$ including the elliptical effects in the second approximation. This supposition leads to the most general form of the final equations because in this case the nonlinear terms are comparable with the term containing the highest derivative of X. In the first approximation we obtain the following problem:

$$\frac{\partial}{\partial X}\left(\frac{\partial^2 \psi_1}{\partial y^2} - R_1(u_0, g_0)\psi_1\right) = D_1(u_0, g_0), \tag{3.2a}$$

$$\psi_1(x,0) = 0, \quad \psi_1'(x,\infty) = 0, \tag{3.2b, c}$$

$$u_1 = \frac{\partial \psi_1}{\partial y}, \quad v_1 = -\frac{\partial \psi_1}{\partial X}, \quad g_1 = \frac{2yg_0''}{u_0} X + \frac{g_0'}{u_0}\psi_1, \tag{3.2d–f}$$

$$p_1 = -\int_y^\infty \frac{1}{2\eta^2} g_0 g_1 \, \mathrm{d}\eta. \tag{3.2g}$$

The general solution of (3.2) is

$$\psi_1 = X\phi_{20}(y) + A(X)\phi_0(y), \tag{3.3}$$

where $A(X)$ is an arbitrary function, which will be determined by the condition of solvability of the second approximation; and ϕ_0 is the solution of the problem

$$\phi_0'' - R_1(u_0, g_0)\phi_0 = 0, \quad \phi_0(0) = 0, \quad \phi_0'(\infty) = 0, \tag{3.4a–c}$$

with normalization $\phi_0'(0) = 1$. This solution exists because the u_0, g_0 profiles correspond to a critical state. The function $\phi_{20}(y)$ is a solution of the problem

$$\phi_{20}'' - R_1(u_0, g_0)\phi_{20} = D_1(u_0, g_0), \quad \phi_{20}(0) = 0, \quad \phi_{20}'(\infty) = 0. \tag{3.5a–c}$$

A solution of ϕ_{20} exists because we consider that u_0, g_0 correspond to a bifurcation point and that the condition (2.7) is satisfied.

In the first approximation, the vortex core produces a displacement in the external potential flow:

$$v_1(X,\infty) = -\phi_{20}(\infty) - A'(X)\,\phi_0(\infty) + o(\exp). \tag{3.6}$$

This displacement is taken into account in the boundary conditions for u_2 as $y \to \infty$. Using (3.6), (3.1) and (2.1) we find that as $y \to \infty$

$$u_2(X,y) = \frac{\epsilon^2}{\theta^3}\phi_0(\infty)\left[\left(\ln\frac{\theta}{\epsilon} + \tfrac{1}{2}\ln 2 - \tfrac{1}{2}\ln y\right)A''(X) + \tfrac{1}{2}L(A'''(\lambda), X)\right] + o(1), \tag{3.7a}$$

$$L(A'''(\lambda), X) = \int_{-\infty}^{+\infty} A'''(\lambda)\ln|X-\lambda|\,\operatorname{sgn}(X-\lambda)\,\mathrm{d}\lambda. \tag{3.7b}$$

Taking the limit $\epsilon \to 0$ in the Navier–Stokes equations we obtain a system of equations for the second approximation. The term

$$\frac{\epsilon^3}{\theta^3}\frac{1}{2y}u_0\frac{\partial v_1}{\partial X}$$

is preserved in the normal momentum equation because it is responsible for the elliptical effects.

After substitution of (3.3) and simple manipulation, an equation for ψ_2 is obtained:

$$\frac{\partial}{\partial X}\left(\frac{\partial^2\psi_2}{\partial y^2} - R_1\psi_2\right) = \phi, \tag{3.8a}$$

$$\phi = \frac{\partial}{\partial X}\left[\tfrac{1}{2}R_2(\phi_{20}^2 X^2 + 2X\phi_{20}\phi_0 A + \phi_0^2 A^2) - \frac{\epsilon^2}{\theta^3}\frac{\phi_0}{2y}A''(X) - D_2 X^2\right]$$
$$+ 2XK(\phi_{20}) + 2AK(\phi_0) + D_3(y)\,\phi_0(A - XA'(X)), \tag{3.8b}$$

where functions R_2, D_2, D_3 include only u_0, g_0 profiles and their derivatives; and $K(\phi)$ is a linear differential operator. These functions and the operator $K(\phi)$ are described in the Appendix.

The condition of solvability of (3.8) with boundary conditions $\psi_2(X,0) = 0$, $\partial\psi_2/\partial y \to u_2$ as $y \to \infty$ is

$$\lim_{y\to\infty}\left(\int_0^y \phi\phi_0\,\mathrm{d}y - \phi_0\frac{\partial u_2}{\partial X}\right) = 0. \tag{3.9}$$

We take advantage of arbitrariness in the definition of the parameter θ and, seeking simplicity of the final equation, determine it so that

$$\left.\begin{aligned} \frac{\epsilon^2}{\theta^3}\left(2\ln\frac{\theta}{\epsilon} + \ln 2 + æ\right) &= \frac{|J|}{\phi_0^2(\infty)}, \\ æ = \lim_{y\to\infty}\left(\frac{1}{\phi_0^2(\infty)}\int_0^y \frac{\phi_0^2(\zeta)}{\zeta}\mathrm{d}\zeta - \ln y\right), \\ J = \int_0^\infty R_2\phi_0^3\,\mathrm{d}y. \end{aligned}\right\} \tag{3.10}$$

We then obtain from the solvability condition (3.9) the equation for the unknown function $A(x)$

$$\operatorname{sgn}(J)\frac{\mathrm{d}}{\mathrm{d}X}(A'' + \mu L(A''', X)) = 2(AA' + 2q_1 A + q_2 X + \beta(A - XA')), \tag{3.11}$$

where $\mu = \epsilon^2\phi_0^2(\infty)/\theta^3|J|$; and q_1, q_2, β are constants, which are completely determined

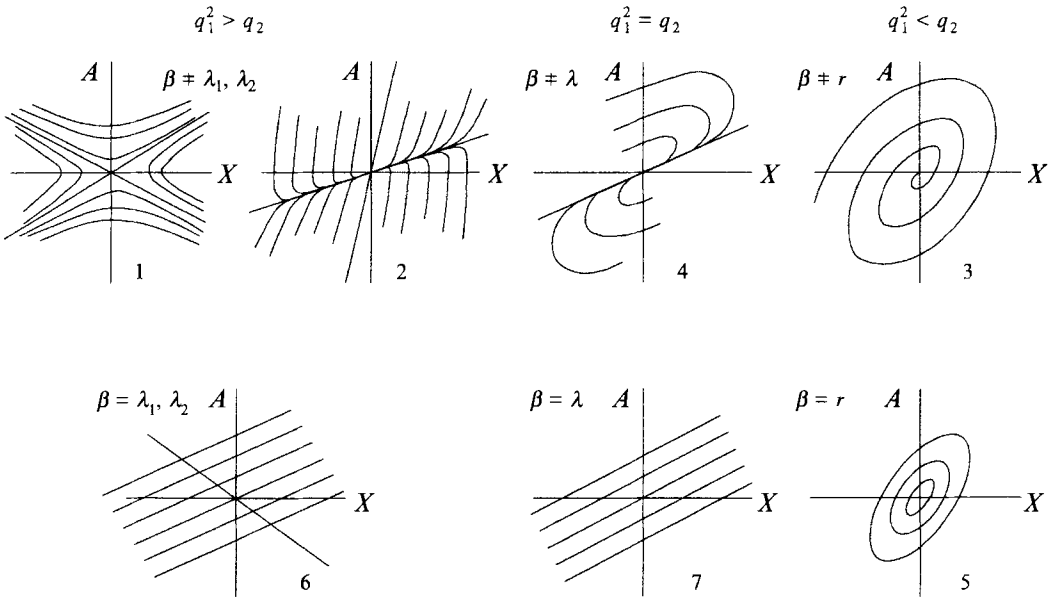

FIGURE 9. Seven possible structures of the solutions of (3.12) near a bifurcation point.

if the u_0, g_0 profiles are known. The procedure for calculation of these constants is described in the Appendix. Equation (3.11) is composite, because $\mu = O(1/\ln(\theta/\epsilon)) \to 0$ as $\epsilon \to 0$, and the term with L should be discarded in the limit. Nevertheless, this term is included in (3.10) because the decline of μ is very slow.

3.2. *Analysis of the bifurcation points in the quasi-cylindrical approximation*

The elliptical effects near a bifurcation point are represented by the terms on the left-hand side of (3.11). If θ is much larger than that determined in (3.10), a small parameter will appear in front of these terms. We shall omit them and analyse the equation describing the solutions of the quasi-cylindrical approximation near a bifurcation point

$$AA' + 2q_1 A + q_2 X + \beta(A - XA') = 0. \tag{3.12}$$

Exactly this equation would be obtained if we were to apply the procedure described above to the quasi-cylindrical approximation system instead of the Navier–Stokes equations.

Equation (3.12) is closely connected with the equations describing the behaviour of a conservative two-dimensional dynamic system near a point of equilibrium. It is possible to introduce new independent variables t, $A(t)$, $X(t)$ and represent (3.12) as the linear system

$$\frac{dA}{dt} = -(2q_1 + \beta)A - q_2 X, \quad \frac{dX}{dt} = A - \beta X.$$

The classification of solutions of this system is well-known and may be found in most books on differential equations (e.g. Arnold 1971).

Equation (3.12) may be integrated after substitution of $A = Xf(X)$, where f is a new unknown function. All solutions of (3.12) may be divided into three main and four degenerate classes. The behaviour of the integral lines $A(X)$ is shown on figure 9.

If $q_1^2 > q_2$, then the equation $\lambda^2 + 2q_1\lambda + q_2 = 0$ has two different real solutions λ_1, λ_2, where $\lambda_1 > \lambda_2$. If, in addition, $\beta \neq \lambda_1$ and $\beta \neq \lambda_2$, the general solution of (3.12) is

$$|A - \lambda_1 X|^{\lambda_1 - \beta} |A - \lambda_2 X|^{\beta - \lambda_2} = C, \tag{3.13}$$

where $C \geqslant 0$ is an arbitrary constant. Two main solution classes appear in this case: saddle-point structure if $\nu = (\beta - \lambda_2)/(\lambda_1 - \beta) > 0$, and nodal-point structure if $\nu < 0$. In the degenerate cases $\beta = \lambda_{1,2}$ all solutions consist of the general solution $A = \lambda_{2,1} X + C$, where C is an arbitrary constant, and a singular solution $A = \lambda_{1,2} X$.

If $q_1^2 < q_2$, then the equation $\lambda^2 + 2q_1\lambda + q_2 = 0$ has two conjugate roots: $\lambda_{1,2} = r \pm is$. The general solution of (3.12) is

$$\frac{r-\beta}{s} \arctan\left(\frac{A - rX}{sX}\right) + \tfrac{1}{2} \ln\left((A - rX)^2 + s^2X^2\right) = C. \tag{3.14}$$

The lines determined by (3.14) may be represented in the plane (ζ, η), $\zeta = sX$, $\eta = A - rX$ in a polar coordinate system $\phi = \arctan(\eta/\zeta)$, $\rho = (\zeta^2 + \eta^2)^{\frac{1}{2}}$ as $\rho = C \exp((\beta - r)\phi/s)$. The integral curves have spirals forms which transform to ellipses at $\beta = r$.

In the intermediate case $q_1^2 = q_2$, $\lambda_1 = \lambda_2 = \lambda$, the general solution may be represented as

$$\ln|A - \lambda X| + (\beta - \lambda)\frac{X}{A - \lambda X} = C. \tag{3.15}$$

This form may also be obtained from (3.13) or (3.14) in the limit $\lambda_1 \to \lambda_2$. This is the degenerate nodal-point structure. In the case $\beta = \lambda$ the solution is $A = \lambda X + C$.

We remember that only two conditions must be satisfied

$$\left(\phi_0'(\infty) = 0 \quad \text{and} \quad \int_0^\infty D_1 \phi_0 \, dy = 0\right)$$

to realize one of these structures near the point $X = 0$. Which structure appears depends on the u_0, g_0 profiles. It is possible that some of the cases considered above should be discarded as unrealistic after investigation of the correlations between q_1, q_2 and β, using their explicit expressions in the Appendix. We did not study this interesting question. Instead we analysed which structures occur at the first and second bifurcation points observed in our numerical solutions.

The evaluation of the constants q_1, q_2, β turned out to be a difficult numerical problem. There are three main sources of numerical inaccuracy. The first is that the integration of (2.5) close to a bifurcation point cannot be of high accuracy, because the matrix which is inverted to find v_i is ill-conditioned there. An interpolation was used to obtain the profiles for which the condition $\phi_0'(\infty) = 0$ is satisfied accurately. The second is that the condition

$$\int_0^\infty D_1 \phi_0 \, dy = 0$$

must also be accurately observed at the same point. We strived for accurate values of $g_{\infty cr}$, but were not able to reach very high accuracy. The third source of inaccuracy is related to the presence of high derivatives in the expressions for q_1, q_2, β. We transformed these expressions by integration by parts so that they included only first and second derivatives.

In spite of this we did not reach the appropriate accuracy in the calculation of some parameters which have small absolute value near the points. Fortunately, these parameters being small does not change the main results and conclusions.

The results of the calculations performed for the first bifurcation point at $\alpha = 0.5$, 1, 1.5 are summarized in table 1. The value of λ_2 is very small at all α and we cannot

α	x_b	$u_0(0)$	$u_0'(0)$	$g_0'(0)$	$\phi_{20}'(0)$	$\phi_0(\infty)$	æ	J	β	λ_1	λ_2	ν
0.5	0.0105	0.413	0.686	0.958	−7.3	0.56	0.23	0.29	6.4	8.1	0	3.7
1.0	0.115	0.482	0.504	0.782	−3.2	0.84	0.05	0.44	2.8	3.1	0.02	9.3
1.5	0.305	0.496	0.334	0.635	−1.95	1.3	−0.31	0.69	1.7	1.9	0.03	8.4

TABLE 1. Results of calculations performed for the first bifurcation point

vouch for its precision. Nevertheless, the precision of ν is quite appropriate. We see that the integral lines $A(X)$ have the saddle-point structure near the first bifurcation point at all α considered.

As $X \to -\infty$ the asymptotic expansion of the solution is

$$A = \lambda_2 X + C(-X)^{-1/\nu} + \ldots. \tag{3.16}$$

The value of the probe function $\phi_0'(X, \infty)$ may be expressed using A:

$$\phi_0'(X, \infty) = Q(A(X) - \beta X), \quad Q = J\theta/\phi_0(0, \infty).$$

The solutions are divided into three groups depending on the value of the arbitrary constant C.

At $C > 0$ the function $\phi_0'(X, \infty)$ is positive everywhere, reaching its minimum at the point

$$X_m = \pm \frac{(\lambda_1 - \lambda_2)\, C^{(\beta-\lambda_2)/(\lambda_1-\lambda_2)}\, |2\beta - \lambda_1 - \lambda_2|^{1/(\lambda_1-\lambda_2)}}{[(\lambda_1 - \beta)^{(\lambda_1-\beta)}\, (\beta - \lambda_2)^{(\beta-\lambda_2)}]^{2/(\lambda_1-\lambda_2)}},$$

where X_m is positive if $\beta > \frac{1}{2}(\lambda_1 + \lambda_2)$ and negative in the opposite case, and approaches the line

$$\phi_0' = Q(\lambda_1 - \beta) X \quad \text{at} \quad X \to +\infty.$$

If $C = 0$, $\phi_0' = Q(\beta - \lambda_2)(-X)$ at $X \leqslant 0$ and can be continued in two ways at $X > 0$: as a regular solution $\phi_0' = Q(\lambda_2 - \beta) X$ or as a singular one $\phi_0' = Q(\lambda_1 - \beta) X$.

At $C < 0$ any solution is terminated at the singular point

$$X_s = \frac{-(-C)^{(\beta-\lambda_2)/(\lambda_1-\lambda_2)}}{[(\lambda_1 - \lambda_2)\, (\lambda_1 - \beta)^{\lambda_1-\beta} (\beta - \lambda_2)^{\beta-\lambda_2}]^{1/(\lambda_1-\lambda_2)}},$$

where $\phi_0'(X, \infty) \sim (X_s - X)^{1/2}$, and cannot be continued beyond it.

We see that the behaviour of the solutions is in agreement with previous numerical and analytical results. Now we can correlate the value of C in (3.16) with the value of $\sigma = g_\infty - g_{\infty cr}$ in the initial conditions. We shall represent the solution of the quasi-cylindrical approximation in the interval $0 \leqslant x \leqslant x_b$ as

$$\psi_d = u_{\infty d}\, r_{0d}^2 (\bar{\psi}_0(x, y) + \sigma \bar{\psi}_1(x, y) + \ldots), \tag{3.17a}$$

$$w_d r_d = u_{\infty d}\, r_{0d} (\bar{g}_0(x, y) + \sigma \bar{g}_1(x, y) + \ldots), \tag{3.17b}$$

where $\bar{\psi}_0(x, y)$, $\bar{g}_0(x, y)$ is the solution at $g_\infty = g_{\infty cr}$ passing point $x = x_b$ regularly.

In the limit $\sigma \to 0$ we obtain the linearized quasi-cylindrical approximation system for the functions $\bar{\psi}, \bar{g}_1$. The solution of this system in singular as $x \to x_b$ and it may be shown that

$$\bar{\psi}_1 = \bar{c}(x_b - x)^{-1/\nu} \phi_0(y) + \ldots,$$

$$\bar{c} = \lim_{X \to X_b} \left[\frac{\partial \bar{u}_1}{\partial x}(x, 0)\, (x_b - x)^{1/\nu} \right],$$

$$\bar{u}_1 = \partial \bar{\psi}_1 / \partial y.$$

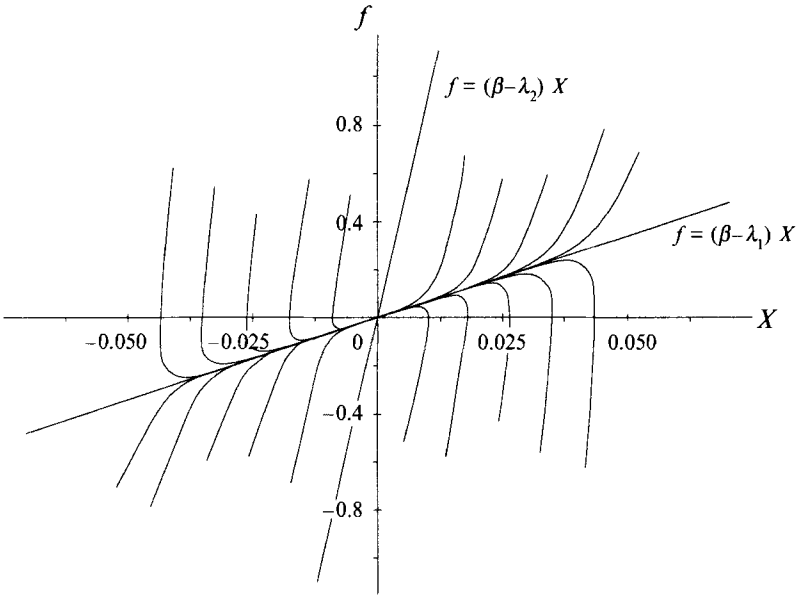

FIGURE 10. The integral lines near the second bifurcation point at $\alpha = 0.5$.

α	x_b	$u_0(0)$	$u_0'(0)$	$g_0'(0)$	$\phi_{20}'(0)$	$\phi_0(\infty)$	æ	J	β	λ_1	λ_2	ν
0.5	0.098	0.0274	0.643	0.304	−2.68	−0.37	0.29	0.57	6.8	—	−85	−13.5
1.0	0.335	0.0331	0.374	0.259	−1.26	−0.35	−0.63	0.34	4.97	—	−139	−29.0
1.5	0.671	0.0342	0.240	0.211	−0.778	−0.46	−1.3	0.38	3.3	—	−105	−32.8

TABLE 2. Results of calculations performed for the second bifurcation point

Matching the expansions (3.1) and (3.17) we find that $C = (g_\infty - g_{\infty cr})\,\bar{c}/\theta^{1+\nu}$. The constant C is contained in the boundary conditions of (3.11). Therefore, the flow near the first bifurcation point described by (3.11) is influenced by the deflection $g_\infty - g_{\infty cr}$ at $|g_\infty - g_{\infty cr}| = O(\theta^{1+\nu})$.

Calculations of q_1, q_2, and β were also performed for the second bifurcation point. The results are presented in table 2. In this case λ_1 is very small at all α and we were not able to ensure its precision; λ_1 is small for the same reason as λ_2 near the first point: $q_2 \ll q_1^2$. This relationship was observed in all cases considered. It is quite possible that $q_2 = 0$ at any bifurcation point, but we did not succeed in proving this. The integral lines have the nodal-point structure near the second bifurcation.

We are able to study the behaviour of the integral lines in detail using (3.13). The picture of the integral curves of $f = Q\phi_0', Q = -J\theta/\phi_0(\infty)$ is schematically represented in figure 10. Two lines, $f = (\beta - \lambda_1)X$ and $f = (\beta - \lambda_2)X$, pass the central point regularly. All curves with initial conditions from the sector $(\beta - \lambda_1)X < f < 0$ at $X < 0$ converge to the line $f = (\beta - \lambda_1)X$ and pass the point $(0, 0)$ along this line. Then the curves spread from the line and fill the sector $0 < f < (\beta - \lambda_2)X$ at $X > 0$. The asymptotic expansion of the solutions near the line $f = (\beta - \lambda_1)X$ at $X > 0$ is

$$f = (\beta - \lambda_1)X + c_f X^{-\nu} + \ldots, \quad A = \lambda_1 X + c_A X^{-\nu} + \ldots, \qquad (3.18a, b)$$

where c_f, c_A are arbitrary constants. The curves may be continued infinitely for

$c_f, c_A \geqslant 0$, but are terminated at singular points X_s for $c_f, c_A < 0$. At these points $\phi_0'(X, \infty) \sim (X_s - X)^{1/2}$ and solution cannot be continued.

The behaviour of the integral curves is in agreement with numerical results. The analysis explains why we were able to pass the point where $\phi_0'(x, \infty) = 0$ regularly and why the numerical solutions of (2.3) are not stable beyond this point.

The problem of continuation of (2.5) for the quasi-cylindrical approximation with the initial conditions stated at the nodal point does not have a unique solution but, instead, an infinite one-parameter class of solutions controlled by the arbitrary constant c_A. The problem is not correct beyond the second bifurcation point and an additional downstream condition is required to provide the uniqueness of the solution. The parabolic equations of the quasi-cylindrical approximation allow the downstream disturbances to propagate upstream.

A similar situation is known for the problem of the hypersonic boundary layer on a flat plate in the strong interaction regime. It was discovered by Neiland (1970) and extended by Brown, Stewartson & Williams (1975) that an eigenfunction $cx^k f(\eta)$ (where x is the distance from the leading edge, η a self-similar variable, c an arbitrary constant, $k > 1$) appears in the asymptotic expansions of the solution near the leading edge, which is the singular point for the problem. The solution of the parabolic boundary-layer equations is not unique and one downstream condition for a scalar quantity must be added. Usually this condition is stated for the downstream pressure. It is possible to change the solution in the whole region from the leading edge to the last downstream position by changing the downstream pressure. Therefore, upstream propagation of the downstream disturbances exists. At present, quite effective numerical methods have been developed to solve these problems.

However, there is a significant difference between the above problem and that considered in this paper. The problem for the hypersonic boundary layer always starts from the singular point at the leading edge and has the property of upstream propagation from the beginning. The present problem concerns the quasi-cylindrical approximation properties which change at the bifurcation point appearing in the process of integration.

Another obstacle which complicates the present problem is that the second bifurcation point is located very close to the point with zero axial velocity on the axis. We know that this point is singular for the axisymmetric wake developing under an unfavourable external pressure gradient and the solution in general cases cannot be continued beyond it (Trigub 1986). The analysis of the quasi-cylindrical approximation solutions near the point with zero axial velocity is a much more difficult one. We have not reached a complete solution yet but we believe that the situation is similar to the one mentioned above. The appearance of the additional degree of freedom at the second bifurcation point changes the situation favourably. We hope to choose the arbitrary constant so that the solution will pass the point of zero axial velocity regularly and the solutions with reversed flows will be obtained just like in the problem of the hypersonic boundary layer.

This hypothesis was confirmed by numerical calculations of the flow beyond the second bifurcation point. The appropriate numerical method to study the solution with the reversed flows and the results are described in the following section.

4. The solutions of the quasi-cylindrical approximation system with large reversed-flow regions

4.1. *Numerical method*

The numerical method was specially constructed to look for regular solutions with reversed-flow regions. We did not have proof that such solutions existed except for the general considerations mentioned above. The scales and space structure of the solutions were unknown. For these reasons the main requirement was not rapidity but high accuracy and ability to find any solutions, even very unstable ones.

The coordinate transformation $\eta = y/\delta(x)$ in the radial direction was performed and the quasi-cylindrical approximation problem was reformulated as follows:

$$\frac{\partial f}{\partial x}\psi' - \frac{\partial \psi}{\partial x}f''' = -\frac{1}{\delta}\frac{g}{2\eta^2}\left(\frac{\partial g}{\partial x} - \frac{1}{\delta}\frac{\mathrm{d}\delta}{\mathrm{d}x}\eta g'\right) + 2(\eta f)'', \tag{4.1a}$$

$$\frac{\partial g}{\partial x}\psi' - \frac{\partial \psi}{\partial x}g' = 2\eta g'', \quad f = \frac{1}{\delta^2}\psi'' \tag{4.1b, c}$$

$$x_0 \leqslant x \leqslant x_1, \quad 0 \leqslant \eta < \infty, \tag{4.1d}$$

$$\psi(x,0) = 0, \quad |f(x,0)| < \infty, \quad g(x,0) = 0, \tag{4.1e}$$

$$\psi'(x,\infty) = \delta, \quad f(x,\infty) = 0, \quad g(x,\infty) = g_\infty, \tag{4.1f}$$

$$\psi(x_0,\eta) = \psi_0(\eta), \quad g(x_0,\eta) = g_0(\eta), \tag{4.1g}$$

where primes denote differentiation with respect to η. Then the flow region was transformed into the standard domain

$$-1 \leqslant \xi \leqslant 1, \quad 0 \leqslant z < \infty, \tag{4.2a}$$

$$x = x_0 + \gamma\frac{1+\xi}{1-\beta\xi}, \quad \beta = 1 - \frac{2\gamma}{x_1 - x_0}, \tag{4.2b, c}$$

$$\eta = C_1 z + C_2 z^\kappa. \tag{4.2d}$$

The pseudo-spectral method was used to calculate x- and y-derivatives at the collocation points. The functions f and g were represented as the finite sums

$$f = \sum_{m=0}^{M}\sum_{n=0}^{N}\hat{f}_{mn}\,T_m(\xi)\,B_n(z), \tag{4.3a}$$

$$g = g_\infty(1 - \mathrm{e}^{-\eta}) + \bar{g}, \tag{4.3b}$$

$$\bar{g} = \sum_{m=0}^{M}\sum_{n=1}^{N}\hat{g}_{mn}\,T_m(\xi)\,H_n(z), \tag{4.3c}$$

where $T_m(\xi) = \cos(m \arccos \xi)$ are the Chebyshev polynomials, $B_n(z) = \mathrm{e}^{-z/2}L_{n-1}(z)$, $H_n(z) = zB_n(z)$, L_n are the Laguerre polynomials, and $\hat{f}_{mn}$, $\hat{g}_{mn}$ are unknown coefficients.

The numerical solution $f_{ij} = f(\xi_i, z_j)$, $\bar{g}_{ij} = \bar{g}(\xi_i, z_j)$ was calculated at the collocation points $\xi_i = \cos(\pi(M-i)/M)$, $i = 0$–M, and $z_j, j = 1$–N, coinciding with zeros of the Laguerre polynomials: $L_N(z_j) = 0$. The x-derivatives at the collocation points were calculated identically for f and $\bar{g}$:

$$\left(\frac{\partial a}{\partial x}\right)_{i,j} = \left(S(\xi)\frac{\partial a}{\partial \xi}\right)_{i,j} = \sum_{l=0}^{M} DX1_{il}\,a_{lj}, \tag{4.4a}$$

$$S(\xi) = \frac{(1-\beta\xi)^2}{\gamma(1+\beta)}, \tag{4.4b}$$

where a_{li} is f_{li} or $\bar{g}_{li}$.

The calculation of first and second η-derivatives was different for f and $\bar{g}$ because of the special form of representation used for $\bar{g}$ which takes into account the boundary condition on the axis $\bar{g}(x,0)=0$:

$$\left(\frac{\partial f}{\partial \eta}\right)_{i,j} = \left(p(z)\frac{\partial f}{\partial z}\right)_{i,j} = \sum_{k=1}^{N} DF1_{jk} f_{ik}, \tag{4.5a}$$

$$p = \frac{1}{C_1 + C_2 \kappa z^{\kappa-1}}, \quad \left(\frac{\partial^2 f}{\partial \eta^2}\right)_{ij} = \sum_{k=1}^{N} DF2_{jk} f_{ik}, \tag{4.5b, c}$$

$$\left(\frac{\partial g}{\partial \eta}\right)_{i,j} = \sum_{k=1}^{N} DG1_{jk}\bar{g}_{ik}, \quad \left(\frac{\partial^2 g}{\partial \eta^2}\right)_{i,j} = \sum_{k=1}^{N} DG2_{jk}\bar{g}_{ik} \tag{4.5d, e}$$

The integral matrices were used to calculate the functions $\partial\psi/\partial\eta$ and $\partial\psi/\partial x$. The integrals were represented as

$$\int_{\eta_j}^{\infty} f(x_i,\tau)\,\mathrm{d}\tau = \sum_{k=1}^{N} RF1_{jk} f_{ik}, \quad \int_0^{\eta_j} \mathrm{d}\lambda \int_{\lambda}^{\infty} f(x_i,\tau)\,\mathrm{d}\tau = \sum_{k=1}^{N} RF2_{jk} f_{ik},$$

and therefore

$$\left(\frac{\partial\psi}{\partial\eta}\right)_{i,j} = \delta_i - \delta_i^2 \sum_{k=1}^{N} RF1_{jk} f_{ik}, \tag{4.6a}$$

$$\left(\frac{\partial\psi}{\partial x}\right)_{i,j} = \delta_i' \eta_j - \sum_{k=1}^{N} RF2_{jk}\left[2\delta_i\delta_i' f_{ik} + \delta_i^2 \sum_{l=0}^{M} DX1_{il} f_{lk}\right], \tag{4.6b}$$

$$\delta_i' = \left(\frac{\mathrm{d}\delta}{\mathrm{d}x}\right)_i. \tag{4.6c}$$

All matrixes $DF1_{jk}$, $DF2_{jk}$, $DX1_{il}$, $DG1_{jk}$, $DG2_{jk}$, $RF1_{jk}$, $RF2_{jk}$ were calculated using standard procedures from the TURLEN Mathematical Library (Blokhin 1992).

Taking into account the representation of the functions, derivatives and integrals, equations (4.1) may be written at the collocation points as a system of $(M+1)\times N$ nonlinear algebraic equations for unknown functions $f_{ij}, \bar{g}_{ij}$, $i = 0$–M, $j = 1$–N. The initial approximation of the solution was usually obtained by extrapolation of the region with smaller x, where the solution was known. Then the standard iterative solver based on the hybrid method of Powell (1970*a*, *b*) from the TURLEN Library was used to solve the nonlinear algebraic system numerically.

4.2. *Numerical results*

The unresolved problem concerning the downstream boundary conditions which provide uniqueness of the solution still exists. It was proved that only one additional downstream boundary condition needs to be stated if the region contains the second bifurcation point and does not contain points with zero or reversed axial velocity. It is not clear what kind of boundary condition is required if the reversed-flow region is not closed and reversed axial velocities occur on the downstream boundary. Nevertheless, if an accurate numerical solution of (4.1), without any additional downstream conditions is obtained, we consider it as one of the possible solutions which correspond to those conditions downstream, which were settled in the iterative process. We are not concerned here with the question of the uniqueness. Instead, we search for some of the solutions numerically which include the reversed-flow regions.

The aim is to prove the existence of regular solutions with large reversed-flow regions and to find regularities among these solutions.

Another general consideration is that singular solutions or solutions with very high gradients cannot be obtained by the numerical method used. Therefore, the numerical procedure acts as a filter which selects the solutions close to the continuation of the separation line $f = (\beta - \lambda_1) X$ in figure 10. The larger the distance $x_1 - x_b$, the smaller is the value of c_A to be chosen to avoid the singularity or high gradients. Extending the region $x_1 - x_b$, we obtain solutions in a narrower region near the continuation of the separating line and as a result this continuation may be found.

The calculations were performed at $\alpha = 0.5$, because in this case the value of $-\nu$ which characterizes the divergence of the integral lines is the smallest. The initial profiles at the upstream boundary $x_0 = 0.1$ were calculated using the numerical method described in §2. The transformation with $\delta(x) = 1 + 4x^2/(0.01 + x)$ turned out to be appropriate and was used in all calculations. The values $c_2 = 0$; $c_1 = 0.2$ for $N = 32$ and $c_1 = 20/z_N$ for $N = 16$; $\gamma = \frac{1}{2}(x_1 - x_0)$ were chosen for the transformations (4.2).

The calculations were performed using two sets of the basic functions: $M = 16$, $N = 16$ and $M = 22$, $N = 32$. The final results presented here were obtained with the second one. The integral invariants (2.8) were calculated at each x_i and their relative error did not exceed 0.1 % for all final results. The initial approximation for the new region (x_0, x_1') was prepared from the solution previously calculated in the interval $x_0 < x \leqslant x_1$ and its linear extrapolation at $x_1 < x \leqslant x_1'$. Primarily, we looked for a solution with a closed region of reversed flow. We were not able to obtain any such solution in spite of numerous attempts using different sequences of the initial approximations.

The results for eight solutions obtained for $x_0 = 0.1$, $x_1 = 0.3$, 0.32, 0.35, 0.4, 0.45, 0.55, 0.8, and 1.0 are shown in figure 11. An important feature is that the solutions on the front portions of intervals have a weak sensitivity to changes of the downstream conditions. The solutions 1, 2, and 3 were obtained with additional downstream condition

$$\frac{\mathrm{d}u}{\mathrm{d}x}(x_1, 0) = 0.$$

An equation must be discarded in the nonlinear algebraic system and substituted by this additional condition. We discarded the equation for circulation at collocation point $M = 1$, $N = 32$. The axial velocity on the axis is represented in figure 11(*a*). The downstream disturbances do not spread far upstream so that all solutions coincide at $x_0 < x < 0.2$. Therefore, the elimination of the equation at the collocation point $M = 1$, $N = 32$ does not change the solution on the front part of the region and gives the opportunity of satisfying the additional condition downstream.

The other solutions 4–8 were obtained without any additional downstream conditions. The axial velocity has, in the solutions 5–8, a minimum and then increases. It might be thought that the closed reversed flow region is formed. However, this conclusion is wrong as can be seen from figures 11(*b*) and 11(*c*) where the vortex thicknesses are shown. These functions increase monotonically. All curves are located in a narrow region and form, where they coincide, a curve, which we consider to be the continuation of the separation line, originating at the second bifurcation point.

The numerical results demonstrate that the equations of the quasi-cylindrical approximation have regular solutions with large reversed-flow regions. In these solutions the axial velocity has a negative minimum inside the reversed-flow region and then increases, still being negative. The vortex radius increases too. On the basis of

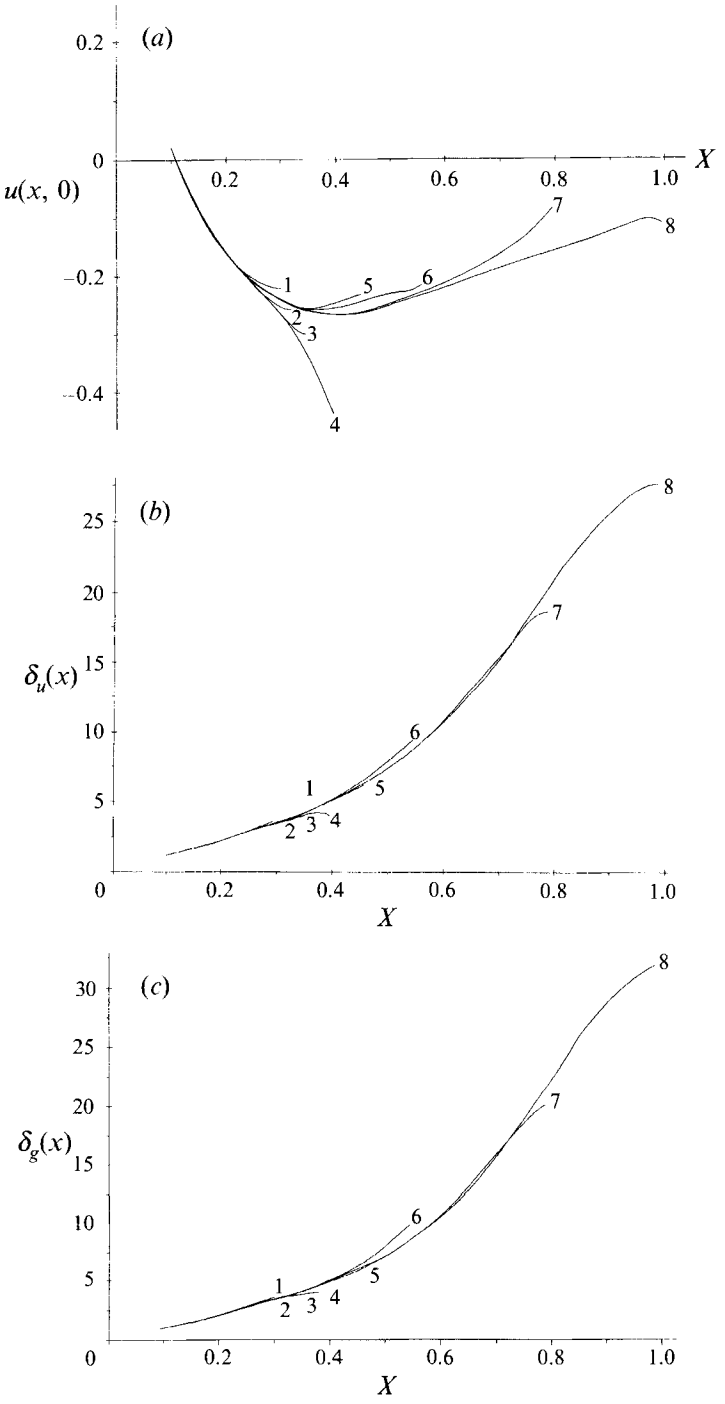

FIGURE 11. (*a*) Velocity on the axis, (*b*) vortex displacement thickness δ_u and (*c*) vortex angular momentum thickness δ_g, for a set of solutions with reversed-flow regions at $\alpha = 0.5$. Solutions 1–8 were obtained at $x_1 = 0.3, 0.32, 0.35, 0.4, 0.45, 0.55, 0.8, 1.0$. The additional downstream condition $\partial u/\partial x\ (x_1, 0) = 0$ was set for solutions 1, 2, 3.

these observations we can suppose that unbounded vortex breakdown with a large almost stagnated region enveloped by the mixing layer may be realized far downstream. The small negative velocity inside the region is induced by the mixing-layer suction. Similar structures were found for boundary-layer separation in supersonic flow by Neiland (1971) and in incompressible fluid by Sychev (1972). We shall investigate this possible application of the quasi-cylindrical approximation.

4.3. *The asymptotic expansions of the solution with unbounded vortex breakdown far downstream*

We shall consider the reversed-flow region to be infinitely expanding as $x \to +\infty$. Suppose that the flow inside the region stagnates as $x \to +\infty$. The region is separated from the external potential flow by the mixing layer whose thickness is small compared with the distance from the axis to the zero streamline situated at $y = \Delta(x)$, $\Delta \to \infty$ as $x \to \infty$. We shall introduce new variables ξ, n to transfer the problem for the axisymmetric mixing layer to a form similar to that for the flat mixing layer

$$x = \int_0^{\xi} \frac{d\xi}{2\Delta}, \quad y = \Delta(\xi) + n. \tag{4.7a, b}$$

Then the equations of the quasi-cylindrical approximation are transformed to the system

$$u\frac{\partial u}{\partial \xi} + V\frac{\partial u}{\partial n} = -\frac{\partial p}{\partial \xi} + \Delta'\frac{\partial p}{\partial n} + \frac{\partial}{\partial n}\left[\left(1+\frac{n}{\Delta}\right)\frac{\partial u}{\partial n}\right], \tag{4.8a}$$

$$u\frac{\partial g}{\partial \xi} + V\frac{\partial g}{\partial n} = \left(1+\frac{n}{\Delta}\right)\frac{\partial^2 g}{\partial n^2}, \quad V = \frac{1}{2\Delta}v - \Delta' u, \tag{4.8b, c}$$

$$\frac{\partial p}{\partial n} = \frac{g^2}{4(\Delta+n)^2}, \quad \frac{\partial u}{\partial \xi} + \frac{\partial V}{\partial n} = 0. \tag{4.8d, e}$$

It will be confirmed below that the asymptotic expansion of the solution in the mixing layer ($n = O(1)$) as $\xi \to \infty$ is

$$\psi = \sqrt{2}(\xi^{1/2} f_0(\eta) + \ln \xi f_1(\eta) + f_2(\eta) + O^*(\xi^{-1/2})), \tag{4.9a}$$

$$g = (g_0(\eta) + \xi^{-1/2} \ln \xi g_1(\eta) + \xi^{-1/2} g_2(\eta) + O^*(\xi^{-1})), \tag{4.9b}$$

$$\eta = \frac{n}{\sqrt{2}\xi^{1/2}}, \quad u = \frac{1}{\sqrt{2}\xi^{1/2}}\frac{\partial \psi}{\partial \eta}, \quad V = -\left(\frac{\partial \psi}{\partial \xi} - \frac{1}{2}\frac{\eta}{\xi}\frac{\partial \psi}{\partial \eta}\right). \tag{4.9c–e}$$

The following problems are obtained in the leading-order approximation:

$$f_0''' + f_0 f_0'' = 0, \quad f_0(0) = 0, \quad f_0'(+\infty) = 1, \quad f_0'(-\infty) = 0, \tag{4.10a–d}$$

$$g_0'' + f_0 g_0 = 0, \quad g_0(+\infty) = g_\infty, \quad g_0(-\infty) = 0. \tag{4.10e–g}$$

The first problem coincides with that of a two-dimensional mixing layer and has the solution $f_0''(0) = 0.587$, $f(-\infty) = -a = -0.876$, $\delta = \lim_{\eta \to +\infty}(\eta - f_0) = 0.374$, and $f_0' \sim e^{a\eta}$ at $\eta \to -\infty$. The solution of the second problem is $g_0 = g_\infty f_0'(\eta)$.

The pressure at $\eta = O(1)$ is found using these solutions:

$$p = p_\infty - \frac{g_\infty^2}{4\Delta} + \frac{g_\infty^2}{2\sqrt{2}}\frac{\xi^{1/2}}{\Delta^2}(f_0''' + f_0 f_0' + \delta) + O\left(\frac{1}{\Delta^2}\right). \tag{4.11}$$

The flow inside the region moves upstream from the stagnated state as $x \to +\infty$ under

the action of the pressure variation (4.11). The viscous effects are negligible in the leading-order approximation. The flow is considered as potential, without circulation, far downstream and, hence, everywhere inside the region. Therefore, the axial velocity inside the region is expressed using Bernoulli's integral:

$$u = -(2(p_\infty - p))^{1/2} = -\frac{g_\infty}{\sqrt{2}\Delta^{1/2}} + \tfrac{1}{2}g_\infty \delta \frac{\xi^{1/2}}{\Delta^{3/2}} + O(\Delta^{-3/2}). \tag{4.12}$$

The function v inside the region is obtained from the equation of continuity:

$$v = -y\left[\frac{g_\infty}{\sqrt{2}}\frac{\Delta'}{\Delta^{1/2}} + \tfrac{1}{2}g_\infty \delta \frac{1}{\xi^{1/2}\Delta^{1/2}}\left(1 - 3\xi\frac{\Delta'}{\Delta}\right) + O(\Delta^{-3/2})\right]. \tag{4.13}$$

The function V near the mixing layer is calculated from (4.12) and (4.13):

$$V = \frac{g_\infty}{2\sqrt{2}}\frac{\Delta'}{\Delta^{1/2}} + O\left(\frac{1}{\xi^{1/2}\Delta^{1/2}}\right). \tag{4.14}$$

On the other hand, this function obtained from the solution of (4.10) as $\eta \to -\infty$ is

$$V = \frac{a}{\sqrt{2}}\xi^{-1/2} + O^*\left(\frac{1}{\xi}\right). \tag{4.15}$$

Matching (4.14) and (4.15) shows the correlations $\Delta = k_1\xi + \ldots, k_1 = 4a^2/g_\infty^2$.

Performing the integration (4.7) we find a very unexpected result:

$$\Delta = k_1 \exp(2k_1(x - x_0)) + \ldots,$$

where x_0 is an unknown constant of the integration. The reversed-flow region expands exponentially far downstream.

We represent the expansion of Δ as $x \to +\infty$ as

$$\Delta = k_1\xi + k_2\xi^{1/2}\ln\xi + k_3\xi^{1/2} + O^*(1), \tag{4.16}$$

where k_2 and k_3 are unknown constants, and consequently

$$\xi = e^{2k_1(x-x_0)} - 2\left[2k_2(x-x_0) + \frac{2k_2 + k_3}{k_1}\right]e^{k_1(x-x_0)} + \ldots,$$

$$\Delta = k_1 e^{2k_1(x-x_0)} - [2k_1k_2(x-x_0) + 4k_2 + k_3]e^{k_1(x-x_0)} + \ldots.$$

The expansion of the axial velocity inside the region of the reversed flow (4.12) may be rewritten using (4.16) as

$$u = -\frac{g_\infty}{\sqrt{2}k_1^{1/2}}\xi^{-1/2} + \frac{g_\infty}{2\sqrt{2}}\frac{k_2}{k_1^{3/2}}\xi^{-1}\ln\xi + \frac{g_\infty}{2k_1^{3/2}}\left(\frac{k_3}{\sqrt{2}} + \delta\right)\xi^{-1} + O^*(\xi^{-3/2}). \tag{4.17}$$

This expression allows boundary conditions for the higher approximations in the mixing layer to be stated:

$$f_1''' + f_0f_1'' + f_0''f_1' = 0, \quad f_1(0) = 0 \quad f_1'(+\infty) = 0, \quad f_1'(-\infty) = 0; \tag{4.18a–d}$$

$$g_1'' + f_0g_1' + f_0'g_1 = 0, \quad g_1(+\infty) = 0, \quad g_1(-\infty) = 0. \tag{4.19e–g}$$

The linear homogeneous problems (4.18) and (4.19) have the eigensolutions

$$f_1 = a_1f_0' + b_1, \quad g_1 = g_\infty c_1 f_0'',$$

where b_1, c_1 are arbitrary constants and $a_1 = -b_1/f_0''(0)$.

We obtain the next approximation

$$f_2''' + f_0 f_2'' + f_0' f_2' = 2(f_0' f_1' - f_0'' f_1) - \sqrt{2}\frac{1}{k_1}(f_0'' \eta)', \tag{4.20a}$$

$$f_2(0) = 0, \quad f_2'(+\infty) = 0, \quad f_2'(-\infty) = -\frac{g_\infty}{\sqrt{2}\, k_1^{1/2}}; \tag{4.20b–d}$$

$$g_2'' + f_0 g_2' + f_0' g_2 = 2(f_0' g_1 - g_0' f_1) - \sqrt{2}\frac{1}{k_1}\eta g_0'', \tag{4.21a}$$

$$g_2(+\infty) = 0, \quad g_2(-\infty) = 0. \tag{4.21b, c}$$

The left-hand sides of (4.18), (4.19), (4.20) and (4.21) are the same. As a result, (4.20) and (4.21) have solutions only if the additional solvability conditions are satisfied. The logarithmic terms were specially included into expansions (4.9) to fulfil these conditions.

We find after integration of (4.20), from $\eta = -\infty$

$$f_2'' + f_0 f_2' = -2b_1 f_0' - \frac{\sqrt{2}}{k_1} f_0'' \eta + \frac{a g_\infty}{\sqrt{2}\, k_1^{1/2}}.$$

Evidently, the boundary condition $f_2'(+\infty) = 0$ can be satisfied only if $b_1 = g_\infty^2/4\sqrt{2}$. Then the solution of (4.20) is

$$f_2' = a_2 f_0'' + g_\infty^2 f_{20}', \quad f_{20}' = \frac{1}{2\sqrt{2}}\left(f_0'' \int_0^\eta \frac{(1-f_0')}{f_0''}\,\mathrm{d}\eta - \frac{f_0'' \eta^2}{a^2}\right),$$

where c_2 is an arbitrary constant. The constant k_2 is determined as a result of matching in the second approximation:

$$k_2 = -(2a)^{1/2}.$$

The expansions under consideration now contain four arbitrary constants: a_2, c_2, k_3 and x_0. Additional information is obtained from calculation of the integral invariants C_1, C_2, (2.8). It may be shown that only terms included in expansions (4.9) and (4.17) participate in the calculation of the integrals (2.8) as $\xi \to \infty$. Performing the integrations we obtain the following relationships:

$$C_2 = \tfrac{1}{4} g_\infty^2 \left(3 + \frac{\delta}{a} - \frac{k_3}{\sqrt{2}\, a} - \ln k_1\right) - \sqrt{2}\, g_\infty^2 (J_1 - 2J_2), \tag{4.22}$$

$$C_1 = -2g_\infty x_0 + \tfrac{1}{2} g_\infty^3 \left(1 + \frac{\delta}{2a} - \frac{k_3}{2\sqrt{2a}}\right) - \sqrt{2}\, g_\infty^3 (J_1 - J_2) - \sqrt{2}\, g_\infty^3 J_3 + \frac{1}{\sqrt{2}} g_\infty (a_2 - c_2), \tag{4.23}$$

$$J_1 = \int_{-\infty}^{+\infty} f_{20}'' \eta \,\mathrm{d}\eta = -0.0815, \quad J_2 = \int_{-\infty}^{+\infty} f_{20}'' f_0 \,\mathrm{d}\eta = -0.155,$$

$$J_3 = \int_{-\infty}^{+\infty} f_0' g_{20} \,\mathrm{d}\eta = -0.147.$$

The integral invariants at $\alpha = 0.5$, $g_\infty = 1.18563$ are $C_1 = 0.889$ and $C_2 = 0.686$. The constant k_3 is determined from (4.22). However, two unknown coefficients of the eigenfunctions in the mixing layer, a_2 and c_2, still remain in the expansions.

The location of the region along the x-axis determined by the constant x_0 would be obtained from (4.23) if the value of $(a_2 - c_2)$ is known. We do not know whether these constants are determined uniquely from the solution of the quasi-cylindrical approximation if the initial profiles before the second bifurcation point are fixed.

Therefore, the question about uniqueness of the solution which has the asymptotic expansion obtained remains unresolved.

In this section only the solutions of the quasi-cylindrical approximation are studied. The solutions expanding exponentially as $x \to \infty$ are not correct asymptotic solutions of the Navier–Stokes equations. The displacement produced by the reversed-flow region $v_d r_d \sim \epsilon u_{\infty d} r_{0d} \Delta$ causes axial velocity perturbations $u_d \sim u_{\infty d} \epsilon^2 \Delta \ln(1/\epsilon)$ in the external flow (2.1). The pressure variations induced by these perturbations become comparable with those induced by the external circulation at

$$\Delta \sim (\epsilon(\ln(1/\epsilon))^{1/2})^{-1}.$$

Hence, the elliptical effects in the external flow must be taken into account at $(x - x_0) \sim \ln(1/\epsilon)$. We consider these effects in the next section.

5. The asymptotic theory of the unbounded vortex breakdown

5.1. *The scales and governing equation*

A diagram showing the different regions emerging in the limit $\epsilon \to 0$ and their dimensional scales is shown in figure 12. The distinctive feature of this structure is that the initial quasi-cylindrical region I and region III where elliptical effects are important have comparable longitudinal scales. These regions are separated by the longer intermediate region II where the reversed flow expands exponentially in accordance with (4.16). The thickness of the mixing layer is constant in this region – an interesting fact caused by the strong spilling. We shall obtain these scales and derive the equation describing the flow in region III.

We represent the asymptotic expansions of the solution in the mixing layer as follows:

$$x_d = r_{0d}(S_0 + S_1 x^*), \quad x^* = \int_1^{\xi^*} \frac{\mathrm{d}\xi}{2\Delta^*(\xi)}, \tag{5.1a, b}$$

$$\tfrac{1}{2} r_d^2 = r_{0d}^2 (S_2 \Delta^*(\xi^*) + S_3 n^*), \quad u_d = u_{\infty d}(u^*(\xi^*, n^*) + \ldots), \tag{5.1c, d}$$

$$v_d r_d = u_{\infty d} r_{0d} \left(\frac{S_2}{S_1} 2\Delta^*(\xi^*) \Delta^{*\prime}(\xi^*) + \frac{S_3}{S_1} 2\Delta^* V^*(\xi^*, n^*) + \ldots \right), \tag{5.1e}$$

$$w_d r_d = u_{\infty d} r_{0d} (g^*(\xi^*, n^*) + \ldots), \quad p_d = \rho_{\infty d} u_{\infty d}^2 \left(p_\infty + \frac{1}{S_2} p^*(\xi^*, n^*) + \ldots \right) \tag{5.1f, g}$$

where ξ^*, n^* are new independent variables and S_0, S_1, S_2, S_3 are unknown scaling factors depending on ϵ. It is supposed that $S_0 \gg S_1 \gtrsim S_2 \gg S_3 \gtrsim 1$ as $\epsilon \to 0$. The zero streamline is situated at $n^* = 0$.

The two-dimensional boundary-layer equations are obtained in the main approximation after substitution of (5.1) into the Navier–Stokes equations in the limit $\epsilon \to 0$, if the conditions are satisfied:

$$S_3^2 = \epsilon S_1 S_2, \quad S_3 \ll S_2, \quad S_2 S_3 \ll S_1^2 \tag{5.2}$$

$$u^* \frac{\partial u^*}{\partial \xi^*} + V^* \frac{\partial u^*}{\partial n^*} = \frac{\partial^2 u^*}{\partial n^{*2}}, \quad u^* \frac{\partial g^*}{\partial \xi^*} + V^* \frac{\partial g^*}{\partial n^*} = \frac{\partial^2 g^*}{\partial n^{*2}} \tag{5.3a, b}$$

$$\frac{\partial u^*}{\partial \xi^*} + \frac{\partial v^*}{\partial n^*} = 0, \quad \frac{\partial p^*}{\partial n} = 0. \tag{5.3c, d}$$

The solution of the equation is

$$u^* = f_0'(\eta^*), \quad g^* = g_\infty f_0'(\eta^*), \quad V^* = \frac{1}{\sqrt{2}} \xi^{*-1/2} (\eta^* f_0' - f_0), \quad \eta^* = \frac{n^*}{(2\xi^*)^{1/2}} \tag{5.4a–d}$$

where f_0 is the similarity solution of the mixing layer problem (4.10).

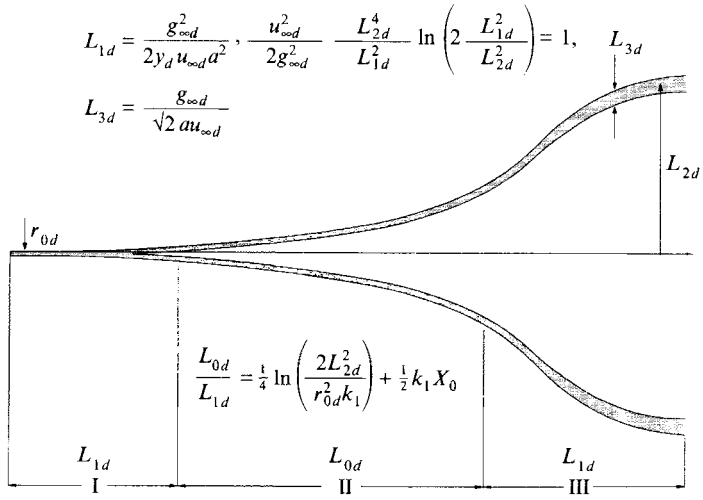

FIGURE 12. The scales and asymptotic structure of unbounded vortex breakdown.

The solution inside the reversed-flow region may be represented as

$$x_d = r_{0d}(S_0 + S_1 x^*), \quad \tfrac{1}{2}r_d^2 = r_{0d}^2(S_2 y_*), \tag{5.5a, b}$$

$$u_d = u_{\infty d}(S_2^{-1/2} u_*(x^*, y_*) + \ldots), \quad v_d r_d = u_{\infty d} r_{0d}\left(\frac{S_2^{1/2}}{S_1} v_*(x^*, y_*) + \ldots\right), \quad w_d = 0, \tag{5.5c–e}$$

$$p_d = \rho_{\infty d} u_{\infty d}^2 \left(p_\infty + \frac{1}{S_2} p_*(x^*, y_*) + \ldots\right). \tag{5.5f}$$

The inviscid thin-layer equations are obtained in the limit $\epsilon \to 0$ as

$$u_* \frac{\partial u_*}{\partial x^*} + v_* \frac{\partial u_*}{\partial y_*} = -\frac{\partial p_*}{\partial x_*}, \quad \frac{\partial p_*}{\partial y_*} = 0, \quad \frac{\partial u_*}{\partial x^*} + \frac{\partial v_*}{\partial y_*} = 0 \tag{5.6a–c}$$

if the condition

$$\epsilon^2 S_1^2 \ll S_2 \ll S_1^2 \tag{5.7}$$

is observed. The solution of (5.6) may be represented as the Bernoulli integral

$$\tfrac{1}{2}u_*^2 + p_* = B(\Psi),$$

where B is arbitrary function of the stream function Ψ.

We consider the motion which originates from the stagnated flow far downstream. Therefore

$$u_* = -[2(p_0 - p_*(x^*)]^{1/2}, \quad v_* = y_* \frac{\mathrm{d}}{\mathrm{d}x^*}[2(p_0 - p_*(x^*))]^{1/2},$$

where p_0 is the stagnation pressure. Using these expressions, we are able to calculate the function V^* and match it with its value obtained from the solution in the mixing layer as $\eta^* \to -\infty$. As a result, the equation which correlates the pressure and the radius of the reversed-flow region is obtained:

$$\frac{1}{2A^*} \frac{S_2^{1/2}}{S_3} \frac{\mathrm{d}}{\mathrm{d}x^*}[A^*(2(p_0 - p_*(x^*))^{1/2}] = \frac{a}{(2\xi^*)^{1/2}}, \tag{5.8}$$

where $a = -f_0(-\infty)$, and $S_2^{1/2}/S_3 = O^*(1)$ is assumed. Equation (5.8) can be integrated using the relationship $d\xi^*/dx^* = 2\Delta^*$:

$$p_* = p_0 - \frac{1}{2\Delta^*}\left(\sqrt{2}\, a \frac{S_3}{S_2^{1/2}} \xi^{*1/2} + q\right)^2, \tag{5.9}$$

where q is the constant of integration.

The displacement produced by the region in the external potential flow is

$$v_d r_d = u_{\infty d} r_{0d} \left(\frac{S_2}{S_1}\frac{d\Delta^*}{dx^*} + \dots\right). \tag{5.10}$$

This displacement causes the longitudinal velocity perturbations which may be calculated in the main approximation using (2.1). Then the pressure perturbations in the external flow near the upper boundary of the mixing layer are found from the Bernoulli equation:

$$p^*(x^*) = \left(\frac{1}{2}\frac{S_2^2}{S_1^2} \ln \frac{2S_1^2}{S_2}\right)\frac{d^2\Delta^*}{dx^{*2}} - \frac{g_\infty^2}{4\Delta^*} - \frac{1}{2}\frac{S_2^2}{S_1^2}\left[\ln \Delta^* \frac{d^2\Delta^*}{dx^{*2}} + \int_{-\infty}^{+\infty} \frac{d^3\Delta^*}{d\lambda^3} \ln |x^* - \lambda| \operatorname{sgn}(x^* - \lambda)\, d\lambda + \frac{1}{2\Delta^*}\left(\frac{d\Delta^*}{dx}\right)^2\right]. \tag{5.11}$$

We assume here that $S_2/S_1 = O^*(1)$. The pressure does not change through the mixing layer in the main approximation. Hence, $p^*(x^*) = p_*(x^*)$, and from (5.9) and (5.11) we obtain an equation correlating Δ^* and ξ^*. Recalling the previous correlation $d\xi^*/dx^* = 2\Delta^*$, we see that a closed system of two equations for Δ^* and ξ^* is obtained.

The scaling

$$\frac{\sqrt{2}\, a S_3}{g_\infty S_2^{1/2}} = 1, \quad \frac{1}{2g_\infty^2}\frac{S_2^2}{S_1^2} \ln\left(\frac{2S_1^2}{S_2}\right) = 1, \quad S_3^2 = \epsilon S_1 S_2, \tag{5.12a–c}$$

$$\mu = \frac{1}{\ln(2S_1^2/S_2)}, \quad \frac{q}{g_\infty} = Q, \quad \frac{2p_0}{g_\infty^2} = \sigma, \quad f = 2\Delta, \quad x = x^*, \quad \xi = \xi^* \tag{5.12d–i}$$

transforms the system into the following:

$$\frac{d^2 f}{dx^2} = \frac{1}{f} - \frac{4}{f^2}(\xi^{1/2} + Q)^2 + \sigma + \mu\left[\frac{d^2 f}{dx^2} \ln \frac{f}{2} + \int_{-\infty}^{+\infty} \frac{d^3 f}{dx^3} \ln |x - \lambda| \operatorname{sgn}(x - \lambda)\, d\lambda + \frac{1}{2f}\left(\frac{df}{dx}\right)^2\right], \tag{5.13a}$$

$$\frac{d\xi}{dx} = f. \tag{5.13b}$$

Now we can be certain that the conditions (5.2) and (5.7) are satisfied.

It requires some effort to get the real dimensional scales of the functions from (5.12), (5.1) and (5.5). in this case we reformulated the expansions (5.1) using (5.12) to make the scaling clear:

$$x_d = L_{0d} + L_{1d} x, \quad r_d = L_{2d} f^{1/2} + L_{3d}(2\xi/f^{1/2})^{1/2} \eta^*, \tag{5.14a, b}$$

$$u_d = u_{\infty d} f_0'(\eta^*) + \dots, \tag{5.14c}$$

$$v_d r_d = u_{\infty d}\left(\frac{L_{2d}^2}{2L_{1d}}\frac{df}{dx} + \frac{L_{2d} L_{3d}}{L_{1d}} \frac{f}{(2\xi)^{1/2}}(\eta^* f_0' - f_0) + \dots\right), \tag{5.14d}$$

$$w_d r_d = g_{\infty d} f_0'(\eta^*) + \dots, \quad p_d - p_{\infty d} = \frac{\rho_{\infty d} g_{\infty d}^2}{L_{2d}^2} p^*(x) + \dots. \tag{5.14e, f}$$

The dimensional scales L_{1d}, L_{2d} and L_{3d} used here do not contain the initial vortex radius r_{0d}:

$$L_{1d} = \frac{g_{\infty d}^2}{2\nu_d u_{\infty d} a^2}, \quad L_{3d} = \frac{g_{\infty d}}{\sqrt{2}\, a u_{\infty d}}, \tag{5.15a, b}$$

$$\frac{u_{\infty d}^2}{2g_{\infty d}^2}\frac{L_{2d}^4}{L_{1d}^2}\ln\left(2\frac{L_{1d}^2}{L_{2d}^2}\right) = 1, \quad \mu = \frac{1}{\ln\left(2L_{1d}^2/L_{2d}^2\right)}, \tag{5.15c, d}$$

$$\sigma = \frac{2(p_{0d}-p_{\infty d})}{\rho_{\infty d} g_{\infty d}^2} L_{2d}^2, \tag{5.15e}$$

where p_{0d} is dimensional stagnation pressure as $x \to +\infty$. The parameter μ is logarithmically small as $\epsilon \to 0$. Only limiting solutions at $\mu = 0$ are considered in this paper.

The solution of (5.13) can be matched with the solution in the intermediate region II only if $Q = 0$. In this case the equations have a solution with asymptotic expansion $f = 4\,\mathrm{e}^{4x} + \ldots$ as $x \to -\infty$.

After matching this solution with the expansion in the intermediate region we find that

$$\frac{L_{0d}}{L_{1d}} = \tfrac{1}{4}\ln\left(\frac{2L_{2d}^2}{r_{0d}^2 k_1}\right) + \tfrac{1}{2}k_1 x_0. \tag{5.16}$$

The value of σ cannot be determined from the matching and is really an essential parameter of the problem.

Note that (5.13) at $\mu = 0$ may be represented as the single differential equation

$$f\frac{\mathrm{d}}{\mathrm{d}\xi}\left(f\frac{\mathrm{d}f}{\mathrm{d}\xi}\right) = \frac{1}{f} - \frac{4\xi}{f^2} + \sigma. \tag{5.17}$$

If the solution of (5.15) is known we can find the corresponding position x_d, velocity u_d and pressure p_d inside the region from the following expressions:

$$x_d = L_{0d} + L_{1d}\int_1^{\xi}\frac{\mathrm{d}\xi}{f(\xi)}, \quad u_d = -\frac{g_{\infty d}}{L_{2d}}\frac{2\xi^{1/2}}{f}, \tag{5.18a, b}$$

$$p_d = p_{\infty d} + \frac{\rho_{\infty d} g_{\infty d}^2}{2L_{2d}^2}\left(\sigma - \frac{4\xi}{f^2}\right). \tag{5.18c}$$

5.2. *Numerical results*

We studied the solution of (5.13) numerically at $\mu = 0$, $Q = 0$. It was convenient to solve the system (5.13) rather than the single equation (5.17). Integration of (5.13) with various initial conditions for f, f', ξ given at some point x demonstrated that three types of solutions exist: monotonically increasing solutions for which $f = \frac{1}{2}\sigma^2 x^2 + \ldots$ as $x \to +\infty$; solutions which are terminated at some singular point $x = x_*$, $\xi = \xi_* + \ldots$, $f = (18\xi_*)^{1/2}\,(x - x_*)^{2/3} + \ldots$ as $x \to x_*$; and, intermediate between these two, monotonically increasing solutions for which $f = 2x/\sigma + \ldots$ as $x \to +\infty$. The third type is the most interesting since solutions of the first type increase too strongly and application of the slender-body potential theory (2.1) is questionable. The singular solutions could be considered using the slender-body theory everywhere, excluding the vicinity of the singular point, but then representation (2.1) must be modified. Therefore, we looked for monotonically increasing solutions for which the stagnation zone has a parabolic form only at a large distance from the point of breakdown ($f \sim 2x/\sigma$).

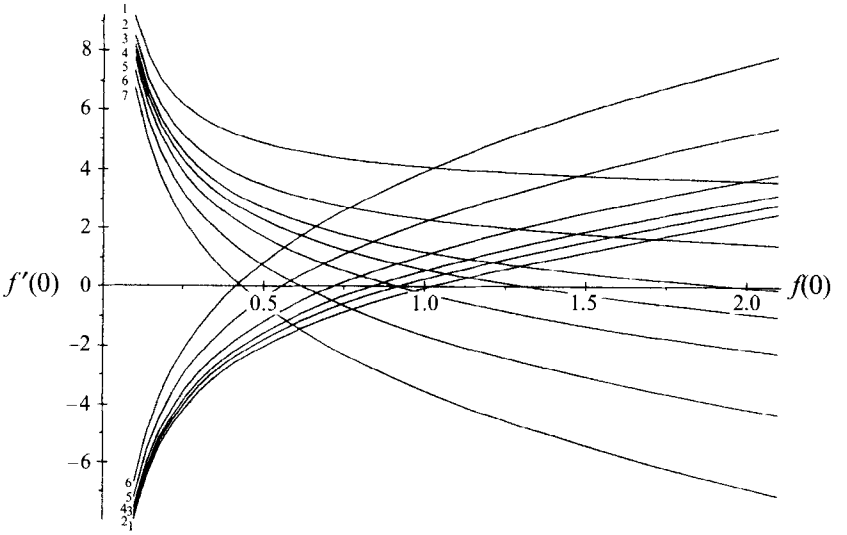

FIGURE 13. The dependence of $f'(0)$ on $f(0)$ for the boundary-value problem (increasing lines 1–6, $\sigma = 1, 2, 3, 5, 10, 20$) and for the initial value problem (decreasing lines 1–7, $\sigma = 0.5, 1, 2, 3, 5, 10, 20$) at which the boundary conditions are satisfied. The points of intersection of the increasing and decreasing curves at the same σ correspond to solutions of the total problem.

The general representation of the solutions with exponential decay as $x \to -\infty$ is

$$f = 4\,e^{4(x-x_0)} + O(e^{8(x-x_0)}) + \exp\left(-\tfrac{1}{16}\,e^{-4(x-x_0)}\right)(c + \ldots), \tag{5.19}$$

where x_0 is an arbitrary translation and c is an arbitrary constant which determines the solution. In principle, all solutions may be obtained starting from $x \ll -1$ and changing the constant c in (5.19). But, in practice, this procedure cannot be realized because the function in front of c decays too strongly as $x \to -\infty$ and all terms in the preceding set of exponents must be determined at $c = O(1)$. Therefore, we used another more reliable procedure to order the solutions.

Since we were searching for monotonically increasing solutions and since the arbitrary translation of the solution in the x-direction is allowed, we supposed that $\xi = 1$ at $x = 0$ without loss of generality. The boundary-value problem for (5.13) was solved at $-\infty < x < 0$ and $f(0) = f_0$, $\xi(0) = 1, f \to 0$ as $x \to -\infty$ at various values of f_0.

The solution was represented as a set of Laguerre polynomials. The spectral collocation method and standard iterative solver from TURLEN Library were used. The dependence of $f'(0)$ on $f(0)$ obtained as a result for $\sigma = 1, 2, 3, 5, 10, 20$ are shown in figure 13 (the increasing curves 1–6 respectively). Then the initial value problem for (5.13) at various $f(0), f'(0)$, $\xi(0) = 1$, $x \geqslant 0$ was studied. The results are also presented in figure 13 (the decreasing curves 1–7 are for $\sigma = 0.5, 1, 2, 3, 5, 10, 20$ respectively). Each curve divides the plane $(f(0), f'(0))$ into two parts. The initial conditions situated above the curve allow for the first type of solution ($f \sim x^2$ as $x \to +\infty$) and those below the curve result in the singular solution (second type). The initial conditions on the curve produce the solution of the third type ($f \sim x$ as $x \to +\infty$) which we are interested in. Therefore, each intersection of a decreasing curve with an increasing one (at the same σ) indicates the existence of a third-type solution on the whole interval $-\infty < x < +\infty$.

Only one such solution was found for each σ from the interval $1 < \sigma < 20$ considered here. Some solutions for $\sigma = 2$ are presented in figure 14(a). Solutions 1–6

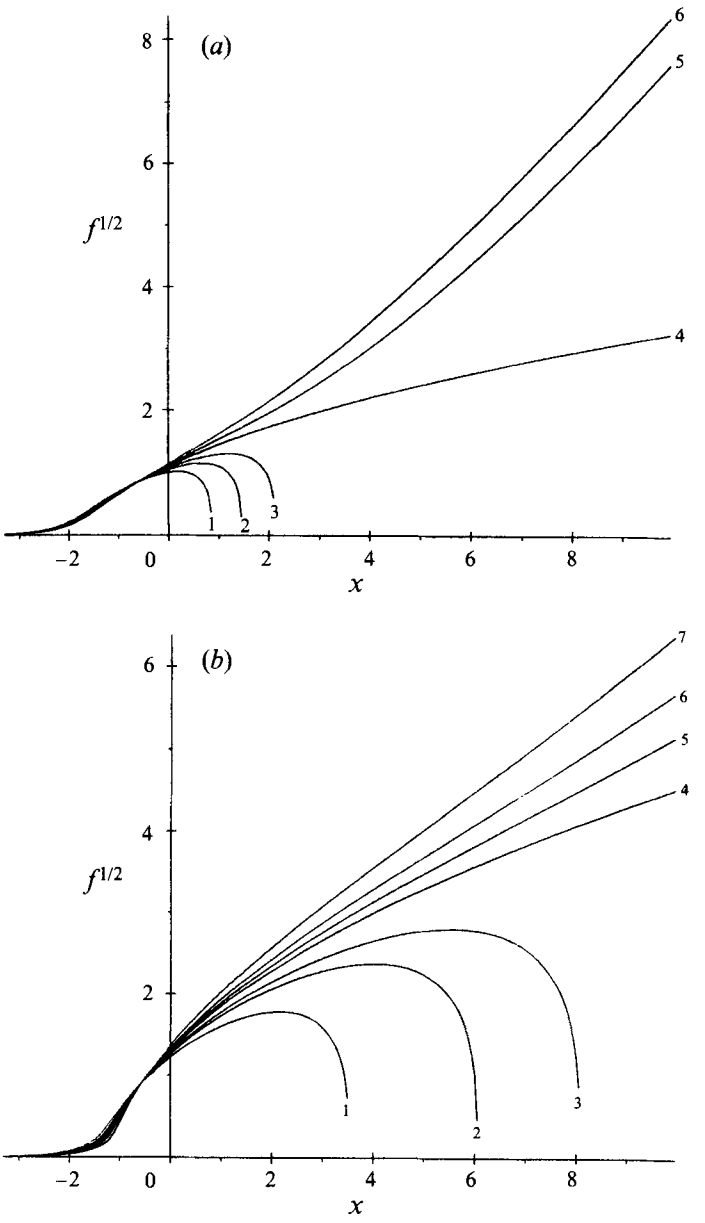

FIGURE 14. The dependence of the radius of stagnation zone on x. (*a*) $\sigma = 2$. The lines 1–6 correspond to $f(0) = 1, 1.1, 1.15, 1.208\,37, 1.25, 1.3$. (*b*) As (*a*) but for $\sigma = 1$. Lines 1–7 correspond to $f(0) = 1.5, 1.6, 1.64, 1.712, 1.75, 1.8, 1.9$. In (*a*) and (*b*) line 4 shows the solution which expands parabolically far downstream.

were obtained for $f(0) = 1, 1.1, 1.15, 1.208\,37, 1.25, 1.3$ respectively. Solution 4 has the required asymptotic expansion $f \sim x$ as $x \to +\infty$ and corresponds with the point of intersection of the curves. Another series of solutions obtained at $\sigma = 1$ is demonstrated in figure 14(*b*). Curves 1–7 correspond to $f(0) = 1.5, 1.6, 1.64, 1.712, 1.75, 1.8, 1.9$ respectively. Vortex breakdown with a parabolically extending stagnation zone is described by curve 4.

It can be seen that a region where the function f increases exponentially is followed by a region where the increase is much more intensive. The intermediate zone between these two regions becomes narrower as σ decreases (compare figures 14(a) and 14(b)). We were not able to obtain a reliable numerical solution of the boundary-value problem mentioned above at small values of σ and $f(0) > 2$. It may be supposed that under these conditions the solution which decays exponentially as $x \to -\infty$ ceases to exist and only solutions which originate from the singular point at some position are possible. This question requires further investigation.

6. Marginal vortex breakdown or transcritical jump?

In this section we shall return to the results obtained in §3 and investigate the asymptotic solutions of the Navier–Stokes equations near the first bifurcation point. The solutions are described by equation (3.11), and only the limiting case $\mu = 0$ will be considered.

If $\beta = \frac{1}{2}(\lambda_1 + \lambda_2)$, equation (3.11) may be integrated and represented as

$$A'' = (A - \lambda_1 X)(A - \lambda_2 X) - C, \tag{6.1}$$

where C is an arbitrary constant. If the additional condition $\lambda_1 = -\lambda_2$ is observed, this equation may be transformed into the form for which the solutions were studied by Trigub (1987) concerning the origin of the recirculation zones in an axisymmetrical wake. However, we shall not consider these particular cases here but instead examine the solutions in a concrete situation, namely near the first bifurcation point at $\alpha = 0.5$. All relevant data are represented in table 1.

It was shown that (3.11) without the highest derivative A''' describes a saddle-point structure of integral lines near the first bifurcation point. The lines of the velocity perturbation on the axis $u(X, 0) = A(X) + \phi'_{20}(0)\, X$ corresponding to this structure at $\alpha = 0.5$ are shown on figure 15. The asymptotic expansion of the solutions as $X \to -\infty$ is

$$A(X) = \lambda_2 X + C(-X)^{-1/\nu} + \ldots, \quad \nu = (\beta - \lambda_2)/(\lambda_1 - \beta), \tag{6.2a, b}$$

and solutions at $C < 0$ are terminated at singular points. More exactly, the solutions at $C = 0, \pm 0.5, \pm 1, \pm 2, \pm 4, \pm 6, \pm 10, \pm 15$ and their symmetrical counterparts are shown in figure 15.

The elliptical effects included in (3.11) through the term A''' change the behaviour of the solutions drastically. A general asymptotic expansion of the solutions as $X \to -\infty$ in this case is

$$A(X) = \lambda_2 X + C(-X)^{-1/\nu}(1 + \ldots) + C_1(-\xi)^r \exp\left(-\tfrac{2}{3}(-\xi)^{3/2}\right)(1 + \ldots) + C_2(-\xi)^r \exp\left(\tfrac{2}{3}(-\xi)^{3/2}\right)(1 + \ldots), \tag{6.3a}$$

$$\xi = (2(\beta - \lambda_2))^{1/3} X, \quad r = -(\tfrac{3}{4} - 1/2\nu). \tag{6.3b, c}$$

The constant C_2 must equal zero for solutions approaching the separation line $A = \lambda_2 X$. Therefore, for each solution at fixed C an additional degree of freedom arises: the deviation of the solution from its quasi-cylindrical approximation which is controlled by constant C_1. However, expansion (6.3) is unsuitable for numerical implementation because the deviation decays very fast as $X \to -\infty$ and all terms of the preceding set must be determined to allow use of it. We used another numerical approach to study the effects of the deviation on the solutions.

First, we fixed position $X_0 < 0$ far enough from point $X = 0$ and solved the boundary-value problem for (3.11) with the following boundary conditions: $A =$

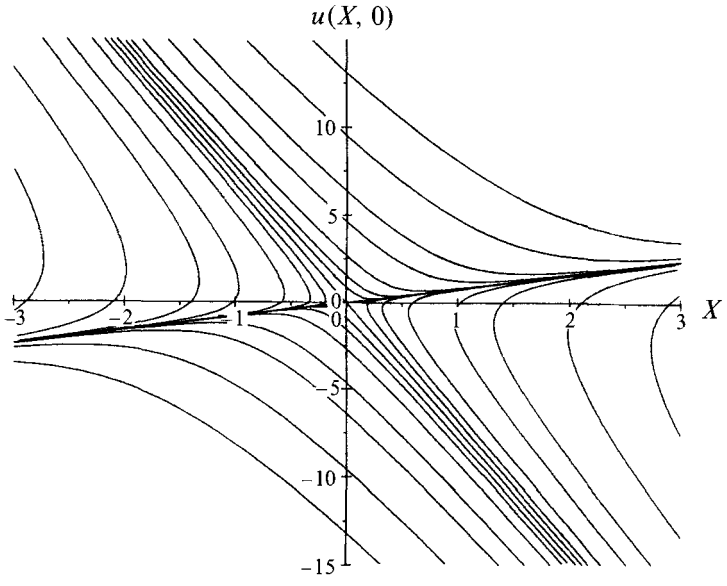

FIGURE 15. The lines of the velocity perturbation $u(X,0)$ near the first bifurcation point at $\alpha = 0.5$, $C = 0, \pm 0.5, \pm 1, \pm 2, \pm 4, \pm 6, \pm 10, \pm 15$.

$\lambda_2 X + C(-X)^{-1/\nu} + \ldots$ at $X = X_1$, $A = A_0$ at $X = X_0$. The deviation was determined by the value of A_0. The region $X_1 < X < X_0$, where $X_1 = -10000$ was chosen and transformed by algebraic transformation (4.2) into the interval $(-1, 1)$ and Chebyshev polynomials were used to represent the solution.

We do not describe the approach in detail because the procedure is quite similar to those discussed above. In this way we were able to obtain the solution of the boundary-value problem for fixed C and A_0, and hence, $A_0'(X_0)$ and $A_0''(X_0)$. then the initial-value problem was solved: equation (3.11) was integrated at $X > X_0$ with initial conditions $A = A_0$, $A' = A_0'$, $A'' = A_0''$ at $X = X_0$. Three types of solutions were observed: the first type of solution tends to infinity ($A \to +\infty$) very fast and cannot be continued far in the X-direction; the second type of solution oscillates strongly and, moreover, the frequency increases as $X \to +\infty$. This second type of solution may be continued far in the X-direction and $u(X,0)$ is negative when X is large enough. Therefore the second type penetrates the region of subcritical flow and may be recognized as transcritical transitions or transcritical jumps (when the transition is far from the smooth transition along the line $A = \lambda_2 X$). This class of solution is fairly wide and we did not find any obstacle to constructing solutions with sharper transitions and more intensive oscillations. As $X \to +\infty$ all these solutions tend (on average) to the separation line $A = \lambda_2 X$. There is also a third type of solution, intermediate between those mentioned above. These solutions approach the regular branch $A = \lambda_1 X$ as $X \to +\infty$.

Some results of calculations obtained at $C = -5$ are shown in figure 16(a). The regular branches $A = \lambda_1 X$, $A = \lambda_2 X$ and a singular solution of the quasi-cylindrical approximation corresponding to $C = -5$ are also presented in the figure. Lines 1 and 2 were obtained for certain deviations prescribed rather arbitrarily. Line 3 originates at $X_0 = -1.8$ and has a negative minimum, approaches the branch $A = \lambda_1 X$ smoothly, and then deviates from this line abruptly into the subcritical region and becomes oscillating. The line was obtained for a particular choice of A_0 which was found by 'shooting'. For A_0 exceeding this value by 10^{-10}, the line almost coincided with the

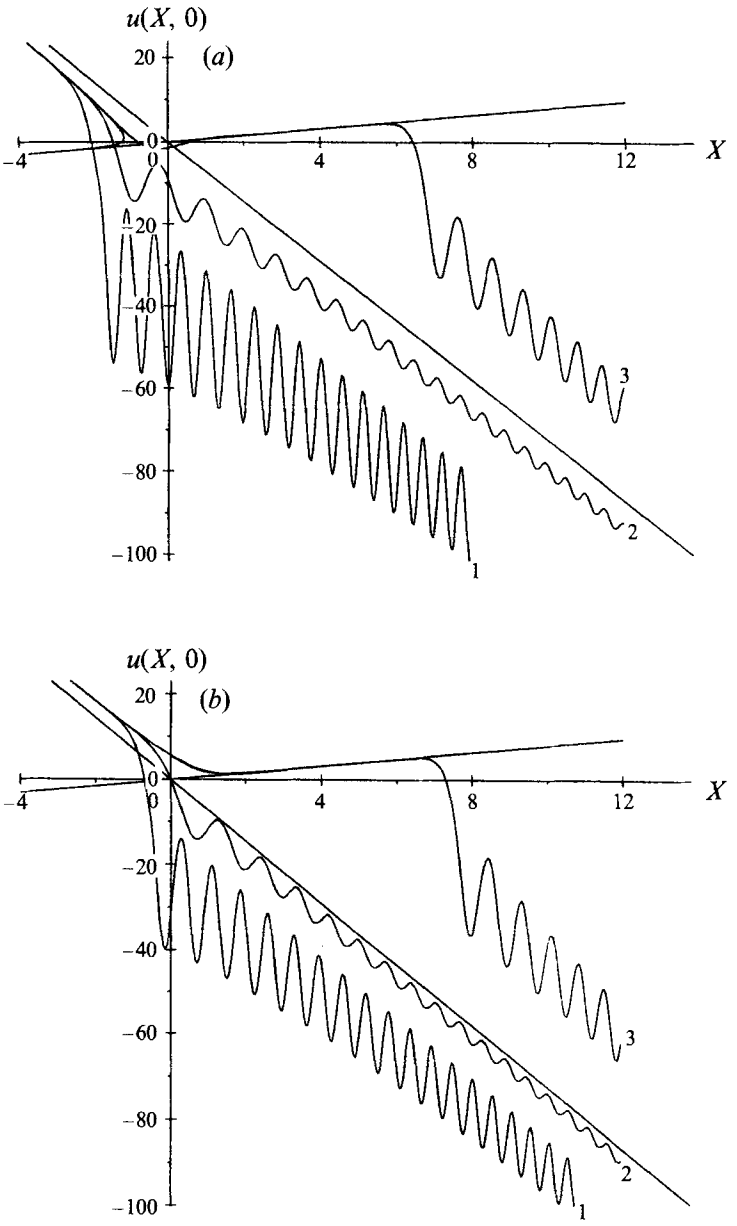

FIGURE 16. (*a*) Velocity perturbation $u(X,0)$ at $C=-5$. The regular branches $A=\lambda_1 X, A=\lambda_2 X$ and singular solution of the quasi-cylindrical approximation are also presented. Lines 1 and 2 correspond to solutions of the second type (transcritical). Line 3 is the solution which is close to the marginal vortex breakdown at $X<4$. (*b*) Velocity perturbation $u(X,0)$ at $C=5$. Lines 1 and 2 correspond to the transcritical solutions. Line 3 is close to the solution of the third type at $X<7$.

previous one at $X \lesssim 4$ and then increased suddenly so that $A \to +\infty$ (this solution is not presented in figure 19). It may be concluded that the solution of the third type approaching the line $A=\lambda_1 X$ as $X \to -\infty$ exists but cannot be produced at large X because of instability of the marching numerical procedure.

Similar results for positive $C=5$ are shown in figure 16(*b*). The most remarkable feature is that the solution of the third type almost coincides with the solution of the

quasi-cylindrical approximation, even at this moderate value of C. Therefore, we believe that at large values of C the elliptical effects do not play any role.

It may be concluded that there are two ways in which the solutions at $C < 0$ which have a singularity and cannot be continued without elliptical effects can, instead, be continued if the following effects are included: transcritical transition when $A \to \lambda_2 X$ as $X \to +\infty$ (second type of solution) and marginal vortex breakdown ($A \to \lambda_1 X$ as $X \to +\infty$, third type). The transcritical transition is not unique – a one-parameter set of such solutions exists at each C. In this paper we do not consider which additional conditions must be stated to determine unique solutions. We think that it may be impossible to formulate physically justified conditions without taking into account the unsteady evolution of the disturbances.

In contrast to this, the solution of the third type was found to be unique for each value of C. First, we attempted to obtain these solutions by 'shooting' starting from some position X_0. However, this method turned out to be unreliable because of strong instability of the marching procedure. Therefore a more reliable method was developed. Two boundary-value problems were solved. The first was for the interval $X_1 \leqslant X \leqslant 0$, $X_1 = -10000$, with boundary conditions $A = \lambda_2 X + C(-X)^{-1/\nu} + \ldots$ at $X = X_1$ and $A''(0) = A_0''$ for fixed C and various A_0''. The algebraic transformation (4.2) was adjusted so that half of the collocation points were situated in $-7 < X < 0$. Finally, $N = 120$ Chebyshev polynomials were used in the solution representation. As a result solutions in the interval $X_1 \leqslant X \leqslant 0$ were obtained and $A_0(0), A_0'(0)$ at various A_0''. The second boundary-value problem was solved in the interval $0 \leqslant X \leqslant 100$ with boundary conditions $A(0) = A_0(0)$, $A'(0) = A_0'(0)$ obtained from the solution of the first problem and $A''(100) = 0$. The parameter of the algebraic transformation was determined so that half of the collocation points belonged to the interval $0 \leqslant X \leqslant 5$, and $N = 64$ Chebyshev polynomials were used. The value $A''(0) = A_1''$ obtained from the solution can then be compared with initial value A_0'' stated in the first problem. We studied $\Delta(A_0'') = A_1'' - A_0''$ looking for zeros which indicate the solutions of the total problem. Using such an indirect method we hoped to find a non-unique solution. Nevertheless, only a unique solution was found at all values of C investigated. This result, however, cannot be considered as mathematical proof of its existence and uniqueness.

A number of solutions are shown in figure 17. Lines 1–6 in figure 17(*a*) correspond to $C = 7, 5, 1, 0, -1, -5, -7$ and line 8 is the solution of the quasi-cylindrical approximation at $C = -7$. At positive $C \geqslant 5$ the elliptical effects have a very small influence. At $C = 0$ the elliptical effects smooth out the sharp bend in the corresponding solution. At $C < 0$ the formation of a retardation zone is observed, and this retardation moves upstream and becomes more intensive as C decreases. The continuation of this process is shown in figure 17(*b*) where lines 1–5 correspond to $C = -9, -11, -13, -15, -17$, while line 6 is the quasi-cylindrical approximation at $C = -17$. The first retardation zone is followed by a zone of acceleration and then the second retardation zone is formed. The results for $C = -19, -21, -23, -25$, are shown in figure 17(*c*) by curves 1–4. At $C = -25$ the second retardation zone is followed by a distinctive zone of acceleration and the formation of the third retardation zone can be observed. We did not meet major obstacles in obtaining the solutions at $C < -25$ except for some difficulties in the numerical calculations. Even at $C = -25$ gradients near the first retardation zone are very high and the collocation points should be condensed there to obtain reliable numerical results at $C < -25$.

The marginal vortex breakdown solutions are interesting because the flow is rather similar to the axisymmetrical forms of vortex breakdown observed in experiments (Harvey 1962; Sarpkaya 1971; Faler & Leibovich 1977). At finite Reynolds numbers,

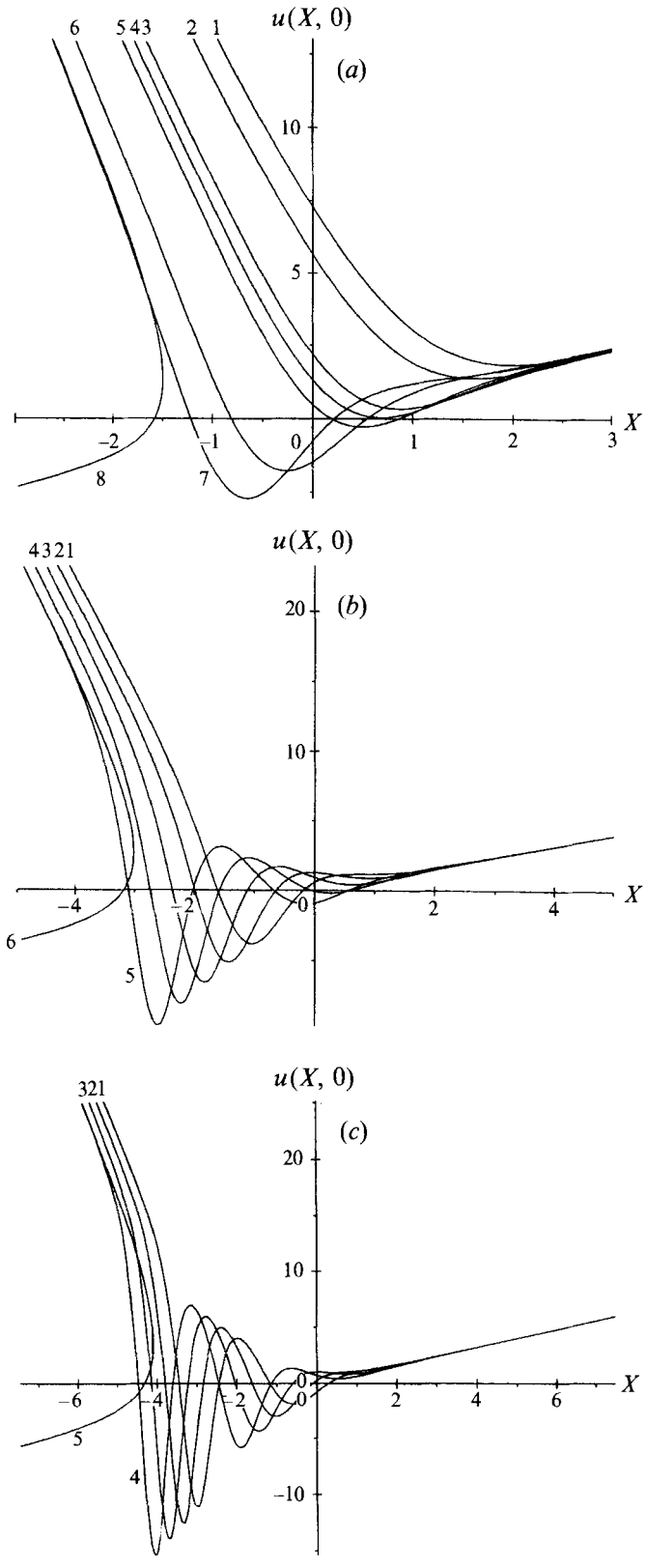

FIGURE 17 (*a–c*). For caption see facing page.

profiles of velocity and circulation can be restored using the function $A(X)$ at (3.2), (3.3). In this way profiles with reversed-flow regions will be obtained at $C \ll -1$. We think that the limits of application of the asymptotic representation may be wide because viscosity effects are taken into account correctly. In any case, these limits could be found by comparing the asymptotic results with results of direct numerical solution of the Navier–Stokes equations for marginal vortex breakdown.

The solutions for marginal vortex breakdown and for transcritical jumps presented above may be considered as different asymptotic representations of real axisymmetrical vortex breakdown. The following questions arise. Which one of these two representations corresponds to the vortex breakdown usually observed in experiments? What is vortex breakdown: transcritical transition or an odd 'bridge' connecting two smoothly developing supercritical portions of the vortex which in no way could be connected smoothly?

7. Conclusions

In this section, we shall critically review some results, present some speculations on possible forms of vortex breakdown, and outline some problems for future investigations.

The aim of this work was to perform a consistent asymptotic study of steady axisymmetrical trailing vortices. This is, of course, a very strong idealization when considering real vortices. However, it is quite justified for a fundamental study since it allows us to find a coherent description of solutions in terms of the parameters, also revealing some singularities. The steady solutions may be used as the base flow in the study of linear stability, or as initial conditions in the study of unsteady nonlinear processes.

Supercritical profiles from the class (2.11) were considered as initial profiles. A criticism concerning this point may be that the initial profiles were chosen too arbitrarily, and the results depend on the choice. However, a justification for this choice is that the experimental profiles may be correlated within this class and that the profiles were used in previous studies (Leibovich 1978). In addition, certain theoretical arguments exist in favour of this choice: the first terms of the expansions (2.9) are described within the class (2.11). However, we recognize the importance of investigating initial profiles created by various vortex generators. This problem of practical concern is far from being properly solved.

Starting from the initial profiles, we attempted to find all the ways in which the flow could be continued infinitely downstream. Numerical investigations of the quasi-cylindrical approximation demonstrated that three kinds of solutions exist in a wide range of parameters: a regular supercritical branch which may be continued infinitely:

$$\text{regular supercritical branch} \rightarrow \text{asymptotic solution of Batchelor}; \tag{7.1}$$

a singular supercritical branch, which is terminated by the singularity of the critical state; and an intermediate solution, which passes the bifurcation point regularly.

One finding of this work is that the latter solution also passes the second bifurcation point regularly and forms an unbounded recirculation zone. The asymptotic analysis

FIGURE 17. Marginal vortex breakdown solutions. (*a*) Lines 1–7 correspond to $C = 7, 5, 1, 0, -1, -5, -7$. Line 8 is the singular solution of the quasi-cylindrical approximation at $C = -7$. (*b*) Lines 1–5 correspond to $C = -9, -11, -13, -15, -17$. Line 6 is the singular solution of the quasi-cylindrical approximation at $C = -17$. (*c*) Lines 1–4 correspond to $C = -19, -21, -23, -25$. Line 5 is the singular solution of the quasi-cylindrical approximation at $C = -25$.

of the solutions near the first bifurcation point revealed a very important fact: the intermediate solution is not a unique one passing into the subcritical region. The regular and singular supercritical branches may also pass through the critical state forming a wave train and approaching the subcritical branch as the wave train is dissipated (§6). Therefore, the following possibilities exist:

$$\left.\begin{array}{l}\text{regular supercritical branch} \longrightarrow \\ \text{singular supercritical branch} \longrightarrow\end{array}\right\} \text{wave train} \longrightarrow \qquad (7.2a)$$

$$\text{subcritical branch} \rightarrow \text{unbounded vortex breakdown.} \qquad (7.2b)$$

The wave train is not uniquely determined; its intensity is a free parameter. It is quite possible that the intensity depends on the history and can be found only from examination of the unsteady process. On the other hand, it may be supposed that a unique choice of the intensity can also be made on the basis of the steady-state analysis by a thorough investigation of the wave train development downstream of the first bifurcation point. The problem has not been solved yet and new ideas are required.

Another important finding of the work is the marginal vortex breakdown:

$$\text{singular supercritical branch} \rightarrow \text{marginal vortex breakdown} \rightarrow \text{asymptotic solution of Batchelor.} \qquad (7.3)$$

This scheme seems very attractive because it is simple and deterministic. It was shown in §6 that the intensity of the intermediate wave is determined uniquely and a solution exists at all values of C within the examined range. However, we must warn here against general conclusions. The problem (3.11) was solved only for particular values of J, β, q_1, q_2 corresponding to $\alpha = 0.5$ and for $-25 \leqslant C \leqslant 7$. We cannot assure that the properties of the solutions will be the same in other conditions. Moreover, we have some reason to suppose that the properties may change drastically. It was shown by Trigub (1987) that the recirculation zones in the axisymmetric wake are described by equation (3.11) at $J > 0$, $\beta = 0$, $\lambda_1 = 1$, $\lambda_2 = -1$. The solutions were thoroughly investigated in a wide range of C. It was found that two solutions exist at $C > C^* = -1.46$ and no solution at $C < C^*$. One of the solutions corresponds to scheme (7.1), while another describes a solitary wave on the regular supercritical branch. The intensity of the wave increases and its length decreases as $C \rightarrow +\infty$. The solutions at high C almost coincide everywhere except in the region where the solitary wave is located. Based on this finding, the solitary wave may be considered as a 'trapped' breakdown. The position and intensity of the 'trapped' wave are determined uniquely; however, its presence is not necessary. If a similar situation occurs for the vortex under certain conditions, it may be characterized by the scheme:

$$\text{regular supercritical branch} \rightarrow \text{'trapped' vortex breakdown} \rightarrow \text{asymptotic solution of Batchelor.} \qquad (7.4)$$

In conclusion, the corresponding problem for (3.11) requires further investigation. The equation proved to be quite general and it is worth a separate work in which its solutions are adequately classified and investigated in a wide range of parameters.

For completeness, we should mention yet another scheme:

$$\text{regular supercritical branch} \rightarrow \text{unbounded vortex breakdown.} \qquad (7.5)$$

This scheme may be considered as a limiting case of (7.4) as the intensity of the trapped bubble increases infinitely. The problem was studied in detail by Trigub (1985*b*) and

developed by Vic. Sychev (1992). The position of the breakdown almost corresponds to the point at which the total pressure on the axis is equal to the pressure in the external flow far from the vortex. The axial velocity drops to zero in the region with axial size comparable with the radius of the vortex, and a parabolic stagnated-flow zone is formed downstream of the region.

We think that schemes (7.1)–(7.5) present a wide foundation for subsequent stability investigations. Actually, each of the schemes will be terminated at some stage by transition to turbulence or by non-axisymmetrical vortex breakdown. It is also possible that some parts of the schemes are globally unstable and will be re-organized if disturbed.

The most interesting candidate for stability analysis seems to be the flow (7.2). The axial velocity gradually decreases to zero and nonlinear effects are revealed at some stages for small perturbations. We suppose that the asymptotic description of non-axisymmetric forms of vortex breakdown may be discovered this way. One interesting issue is the possibility of resonant interaction between the wave train and the small non-axisymmetric disturbances.

Another likely problem for the asymptotic approach is the generalization of the equations describing the flow near the bifurcation points derived in §3.1 to include unsteady effects. The resulting problem statement will be relatively simple and quite productive.

We also feel that the results of the present work might be used to extract correct and interesting problem statements for direct numerical simulations. The direct numerical simulation of vortex breakdown seems a relatively simple and attractive problem because the phenomenon occurs at moderate Reynolds numbers and may be represented as large-eddy motion. However, conceptual difficulties exist concerning the choice and formulation of the problem statement. Asymptotic analysis is actually a tool for elaboration of the problem statements.

Future studies in the directions outlined above would lead to a deeper understanding of complex phenomena in vortex dynamics which are currently inaccurately differentiated and are jointly referred to as 'vortex breakdown'.

We would like to thank INTECO for its support for this work. We would also like to express our special thanks to Carol McHugh for her assistance in preparing the paper for publishing.

Appendix A

Once the profiles $u_0(y)$, $g_0(y)$ at the bifurcation point have been determined, the functions R_2, D_2, D_3, K included in (3.8) may be calculated as follows:

$$R_1 = \frac{u_0''}{u_0} - \frac{g_0 g_0'}{2y^2 u_0^2}, \quad D_1 = \frac{g_0 g_0''}{y u_0^2} - 2\frac{(y u_0')''}{u_0},$$

$$R_2 = \frac{R_1'}{u_0} - \left(\frac{g_0 g_0'}{u_0}\right)' \frac{1}{2y^2 u_0^2}, \quad D_2 = \frac{g_0''^2}{u_0^3} + \frac{g_0}{y u_0^2}\left(y\frac{g_0''}{u_0}\right)'',$$

$$D_3 = \frac{g_0' g_0''}{y u_0^3} + \frac{g_0}{y^2 u_0^2}\left(y\frac{g_0''}{u_0}\right)' + \frac{D_1'}{u_0},$$

$$K(\phi) = \frac{1}{u_0}(y\phi'')'' - \frac{1}{2u_0}(\phi D_1' - \phi' D_1) - \frac{g_0}{2y u_0^2}\left(\frac{g_0'}{u_0}c\right)'' - \frac{g_0}{2y^2 u_0^2}\left[\left(y\frac{g_0''}{u_0}\right)'\phi - y\frac{g_0''}{u_0}\phi'\right] - \frac{1}{y u_0^3} g_0' g_0'' \phi,$$

where the prime denotes differentiation with respect to y. The coefficients β, q_1, q_2 in (3.11) are calculated by integration:

$$J = \int_0^\infty R_2 \phi_0^3 \, dy, \quad \beta J = \int_0^\infty D_3 \phi_0^2 \, dy - \int_0^\infty R_2 \phi_{20} \phi_0^2 \, dy,$$

$$q_1 J = \int_0^\infty R_2 \phi_{20} \phi_0^2 \, dy + \int_0^\infty K(\phi_0) \phi_0 \, dy,$$

$$q_2 J = \int_0^\infty R_2 \phi_{20}^2 \phi_0 \, dy + 2 \int_0^\infty K(\phi_{20}) \phi_0 \, dy - 2 \int_0^\infty D_2 \phi_0 \, dy,$$

where functions ϕ_0, ϕ_{20} are the solutions to (3.4) and (3.5).

REFERENCES

ARNOLD, V. I. 1971 *Ordinary Differential Equations*. Moscow: Nauka.

BATCHELOR, G. K. 1964 Axial flow in trailing line vortices. *J. Fluid Mech.* **20**, 645–658.

BENJAMIN, T. B. 1962 Theory of the vortex breakdown phenomenon. *J. Fluid Mech.* **14**, 593–629.

BLOKHIN, A. B., GRUBIN, S. E., SIMAKIN, I. N. & TRIGUB, V. N. 1992 *TURLEN Library*. INTECO srl, Frosinone, Italy.

BROWN, S. N., STEWARTSON, K. & WILLIAMS, P. G. 1975 Hypersonic self-induced separation. *Phys. Fluids* **18**, 633–639.

FALER, J. H. & LEIBOVICH, S. 1977 Disrupted states of vortex flow and vortex breakdown. *Phys. Fluids* **20**, 1385–1400.

GARTSHORE, I. S. 1963 Some numerical solutions for the viscous core of an irrotational vortex. *NRC Can. Aero. Rep.* LR-378.

GOLDSTEIN, S. 1960 *Lectures on Fluid Mechanics*. Interscience Publ.

HAFEZ, M., AHMAD, J., KURUVILA, G. & SALAS, J. D. 1987 Vortex breakdown simulation. *AIAA Paper* 87–1343.

HALL, M. G. 1967 A new approach to vortex breakdown. *Proc. 1967 Heat Transfer Fluid Mech. Inst.* pp. 319–340. Stanford University Press.

HALL, M. G. 1972 Vortex breakdown. *Ann. Rev. Fluid Mech.* **4**, 195–218.

HARVEY, J. K. 1962 Some observation of the vortex breakdown phenomenon. *J. Fluid Mech.* **14**, 585–592.

LEIBOVICH, S. 1970 Weakly nonlinear waves in rotating fluids. *J. Fluid Mech.* **42**, 803–822.

LEIBOVICH, S. 1978 The structure of vortex breakdown. *Ann. Rev. Fluid Mech.* **10**, 221–246.

LEIBOVICH, S. 1984 Vortex stability and breakdown: survey and extension. *AIAA J.* **22**, 1192–1206.

LEIBOVICH, S. & KRIBUS, A. 1990 Large-amplitude wavetrains and solitary waves in vortices. *J. Fluid Mech.* **216**, 459–504.

LESSEN, M. & PAILLET, F. 1974 The stability of a trailing line vortex. Part 2. Viscous theory. *J. Fluid Mech.* **65**, 769–779.

LESSEN, M., SINGH, P. I. & PAILLET, F. 1974 The stability of a trailing line vortex. Part 1. Inviscid theory. *J. Fluid Mech.* **63**, 753–763.

MAGER, A. 1971 Incompressible, viscous, swirling flow through a nozzle. *AIAA J.* **9**, 649–655.

MAGER, A. 1972 Dissipation and breakdown of a wing-tip vortex. *J. Fluid Mech.* **55**, 609–628.

MORTON, B. R. 1969 The strength of vortex and swirling core flows. *J. Fluid Mech.* **38**, 315–333.

NEILAND, V. YA. 1970 Upstream propagation of the disturbances in interacting hypersonic boundary layer. *Izv. Akad. Nauk, SSSR, Mekh. Zhid. i Gaza*, No. 4, 40–49.

NEILAND, V. YA. 1971 The flow past the separation point at supersonic speed. *Izv. Akad. Nauk SSSR, Mekh. Zhid. i Gaza*, No. 3, 19–25.

PECKHAM, D. H. & ATKINSON, S. A. 1957 Preliminary results of low speed wind tunnel tests on a Gothic wing of aspect ratio 1.0. *Aeronaut. Res. Counc.*, CP 508.

POWELL, M. J. D. 1970*a* A hybrid method for nonlinear equations. In *Numerical Methods on Nonlinear Algebraic Equations*, pp. 87–114. Gordon and Breach.

POWELL, M. J. D. 1970*b* A Fortran subroutine for solving systems of nonlinear algebraic equations. In *Numerical Methods on Nonlinear Algebraic Equations*, pp. 115–161. Gordon and Breach.

RANDALL, J. D. & LEIBOVICH, S. 1973 The critical state: a trapped wave model of vortex breakdown. *J. Fluid Mech.* **53**, 495–515.

SARPKAYA, T. 1971 On stationary and travelling vortex breakdown. *J. Fluid Mech.* **45**, 545–559.

SYCHEV, V. V. 1972 On laminar separation. *Izv. Akad. Nauk SSSR, Mekh. Zhid. i Gaza*, No. 3, 47–59.

SYCHEV, VIC. V. 1992 Asymptotic theory of the vortex breakdown. *Izv. Akad. Nauk Russ., Mekh. Zhid, i Gaza* (to appear).

TRIGUB, V. N. 1985*a* The problem of the vortex breakdown. *Prikl. Matem. i Mekh.*, No. 2, 220–226.

TRIGUB, V. N. 1985*b* The problem of the vortex breakdown in inviscid fluid. *Uchenye Zap. TsAGI*, No. 3, 100–104.

TRIGUB, V. N. 1986 An analysis of the flow near the stagnation point in an axisymmetrical wake. *Izv. Akad. Nauk SSSR, Mekh. Zhid. i Gaza*, No. 2, 53–59.

TRIGUB, V. N. 1987 Asymptotic theory of the origination of recirculation zones in an axisymmetrical wake. *Izv. Akad. Nauk SSSR, Mekh. Zhid. i Gaza*, No. 5, 54–60.